materials

MDPI

Review

Ceramic-Based Dielectric Materials for Energy Storage Capacitor Applications

Srinivas Pattipaka [1], Yeseul Lim [1], Yong Hoon Son [1], Young Min Bae [1], Mahesh Peddigari [2] and Geon-Tae Hwang [1,*]

[1] Department of Materials Science and Engineering, Pukyong National University, 45, Yongso-ro, Nam-Gu, Busan 48513, Republic of Korea; cnuphy444@gmail.com (S.P.); yesle912@naver.com (Y.L.); mike4009@pukyong.ac.kr (Y.H.S.); dud1560@pukyong.ac.kr (Y.M.B.)

[2] Department of Physics, Indian Institute of Technology Hyderabad, Kandi 502284, Telangana, India; mahesh.p@phy.iith.ac.in

* Correspondence: gthwang@pknu.ac.kr

Abstract: Materials offering high energy density are currently desired to meet the increasing demand for energy storage applications, such as pulsed power devices, electric vehicles, high-frequency inverters, and so on. Particularly, ceramic-based dielectric materials have received significant attention for energy storage capacitor applications due to their outstanding properties of high power density, fast charge–discharge capabilities, and excellent temperature stability relative to batteries, electrochemical capacitors, and dielectric polymers. In this paper, we present fundamental concepts for energy storage in dielectrics, key parameters, and influence factors to enhance the energy storage performance, and we also summarize the recent progress of dielectrics, such as bulk ceramics (linear dielectrics, ferroelectrics, relaxor ferroelectrics, and anti-ferroelectrics), ceramic films, and multilayer ceramic capacitors. In addition, various strategies, such as chemical modification, grain refinement/microstructure, defect engineering, phase, local structure, domain evolution, layer thickness, stability, and electrical homogeneity, are focused on the structure–property relationship on the multiscale, which has been thoroughly addressed. Moreover, this review addresses the challenges and opportunities for future dielectric materials in energy storage capacitor applications. Overall, this review provides readers with a deeper understanding of the chemical composition, physical properties, and energy storage performance in this field of energy storage ceramic materials.

Keywords: ceramic-based dielectric materials; polarization; breakdown strength; recoverable energy density; energy efficiency; energy storage capacitors

Citation: Pattipaka, S.; Lim, Y.; Son, Y.H.; Bae, Y.M.; Peddigari, M.; Hwang, G.-T. Ceramic-Based Dielectric Materials for Energy Storage Capacitor Applications. *Materials* **2024**, *17*, 2277. https://doi.org/10.3390/ma17102277

Academic Editor: Georgios C. Psarras

Received: 8 April 2024
Revised: 1 May 2024
Accepted: 8 May 2024
Published: 11 May 2024

1. Introduction

Energy storage devices such as batteries, electrochemical capacitors, and dielectric capacitors play an important role in sustainable renewable technologies for energy conversion and storage applications [1–3]. Particularly, dielectric capacitors have a high power density (~10^7 W/kg) and ultra-fast charge–discharge rates (~milliseconds) when compared to electrochemical capacitors and batteries (Figure 1b) [2–13]. These advantages of dielectric capacitors make them promising for applications in power electronics and pulsed power systems, as shown in Figure 1a. For instance, more than three trillion multilayer ceramic capacitors (MLCCs) are manufactured annually and are used in cell phones or electric vehicles [6–9,14,15]. However, dielectric capacitors have a lower energy storage density of 10^{-2} to 10^{-1} Wh/kg than electrochemical capacitors and batteries, which limits their practical applications. Therefore, high-performance dielectric materials in terms of high energy storage density, high energy efficiency, fast charge–discharge capabilities, better thermal or frequency stability, fatigue resistance, lifetime reliability, equivalent series resistance, and low manufacturing costs are needed for power electronics and pulse power applications.

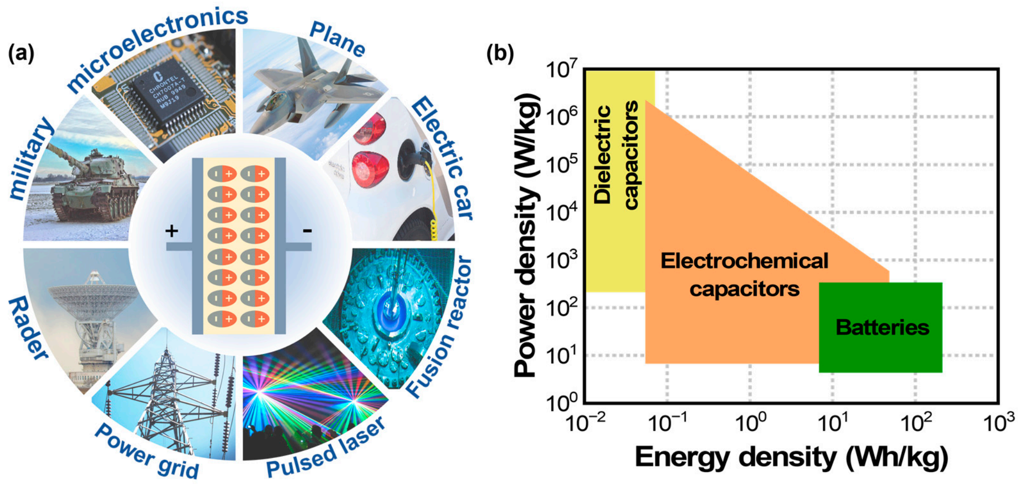

Figure 1. (**a**) Various applications of dielectric capacitors in power electronics and pulse power applications. (**b**) Comparison of the power density versus energy density of batteries, electrochemical capacitors, and dielectric capacitors.

The storage performance depends on the charge accumulation in dielectric materials, which are a key component of capacitors. Dielectric materials, including organic (polyvinylidene fluoride (PVDF), biaxially oriented polypropylene (BOPP), polyimide (PI), etc.), and inorganic (ceramics, glass, and glass-based ceramics) materials, have been widely investigated to improve the energy storage performance [9,16–20]. In recent years, significant improvements to dielectric materials have been made, although each material still has limitations. The polymers offer a high breakdown strength (BDS), low relative dielectric permittivity, and weak thermal stability, making dielectric materials for energy storage a long-term goal. Meanwhile, ceramic-based dielectric materials are popular research topics due to their application in energy storage, adaptability to various environments, fundamentality, and other factors. Therefore, the topic of dielectrics will be discussed further in this review. These materials are classified into linear dielectrics (LDs), ferroelectrics (FEs), antiferroelectrics (AFEs), and relaxor ferroelectrics (RFEs) [17,20]. They are considered viable candidates for energy storage due to their differing properties in BDS and polarization, which primarily influence energy storage performance.

This review paper presents fundamental concepts of energy storage in dielectric capacitors, including an introduction to dielectrics and key parameters to enhance energy storage responses. We also summarize recent progress in dielectrics, such as bulk ceramics, ceramic films, and multilayer ceramic capacitors, including the phase, local structure, microstructure, domain evolution, layer thickness, stability, and electrical homogeneity; fabrication methods, dopants/composites, and various strategies for enhancing energy storage properties in dielectric capacitors are also briefly discussed.

2. Fundamental Concepts for Energy Storage in a Dielectric Capacitor

2.1. Dielectric Capacitor

A parallel plate capacitor is composed of two parallel conducting plates that are separated by a ceramic layer, as schematically shown in Figure 2. When a dielectric capacitor is placed in an external electric field, the electric dipoles will be displaced and oriented due to polarization (Figure 2b). The capacitance of a dielectric capacitor (C) is the ability to store electric charge and is given by the following equation:

$$C = \frac{Q}{V} \quad (1)$$

where Q is the charge and V is the voltage applied to the capacitor.

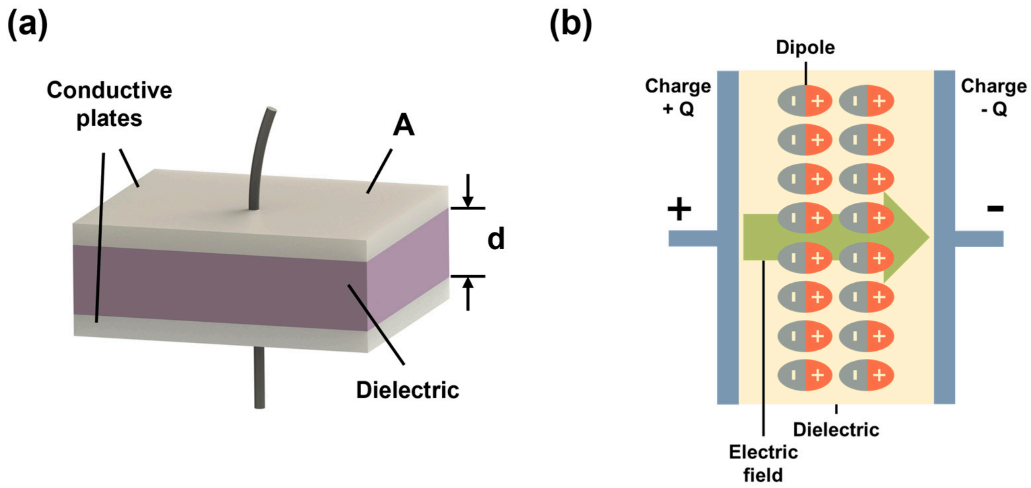

Figure 2. Schematic diagram of (**a**) a dielectric capacitor, and (**b**) a dielectric between two conductive plates, where electric dipoles are displaced and oriented by the applied electric field due to polarization.

According to Gauss's law,

$$V = \frac{Qd}{\varepsilon_0 \varepsilon_r A} \tag{2}$$

The capacitance of a parallel plate capacitor can be calculated in terms of the sample area and thickness via comparing Equations (1) and (2).

$$C = \varepsilon_0 \varepsilon_r \frac{A}{d} \tag{3}$$

where ε_0 is the permittivity of free space, ε_r is relative dielectric permittivity, A is the area of metal plates, and d is the thickness of the ceramic sample (Figure 2a).

2.2. Evaluation of Energy Storage Performance

The energy storage density (W) of a linear dielectric material is determined with the following equation [21]:

$$W = \frac{1}{2} \varepsilon_0 \varepsilon_r E^2 \tag{4}$$

where ε_0 is the permittivity of free space, ε_r is dielectric permittivity, and E is the applied electric field. In contrast, the nonlinear dielectric materials (FEs, AFEs, and RFEs) exhibit energy loss. Therefore, the total energy storage density (W_{tot}), recoverable energy density (W_{rec}), and energy storage efficiency (η) of these materials are calculated from the hysteresis loops as follows [22–24]:

$$W_{tot} = \int_0^{P_m} EdP \text{ (Charging)} \tag{5}$$

$$W_{rec} = \int_{P_r}^{P_m} EdP \text{ (Discharging)} \tag{6}$$

$$\eta = \frac{W_{rec}}{W_{rec} + W_{loss}} \times 100\% \tag{7}$$

where E is the applied electric field, P is polarization, P_{max} is maximum polarization, P_r is remnant polarization, and W_{loss} is energy loss, as schematically shown in Figure 3.

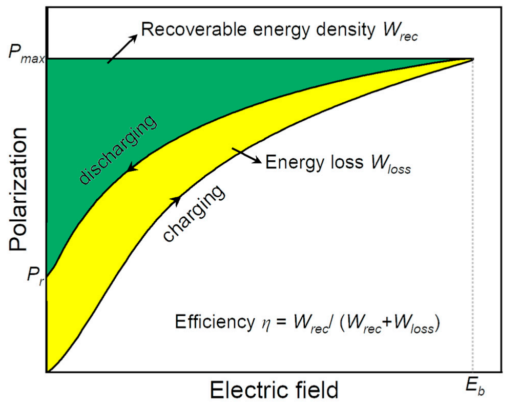

Figure 3. Schematic of the recoverable energy density and energy loss from the *P-E* hysteresis loop of a ceramic capacitor.

2.3. Key Parameters for Energy Storage Performance

2.3.1. Energy Storage Density and Efficiency

W_{rec} and η are the most important parameters for evaluating the energy storage performance of dielectric materials, which are related to dielectric permittivity and polarization. A high W_{rec} of dielectric materials means that more energy can be stored in a given volume, promoting miniaturization and lightweight and low-cost materials being utilized in consumer power electronics and pulse power systems. It can be concluded from Equations (4)–(7) and Figure 3 that a higher ε_r, $P_{max,}$ and BDS lead to higher energy density, whereas low dielectric or hysteresis losses and low P_r improve energy storage efficiency in dielectric materials. Moreover, the material should have low electronic or ionic conductivity to resist higher electric fields.

2.3.2. Polarization Difference

The energy storage density and efficiency of a ceramic capacitor's are mostly related to the shape of the *P-E* loop due to the area under the curve providing the W_{rec} (Figure 3). Therefore, the energy storage performance depends on the value of ΔP ($\Delta P = P_{max} - P_r$), and the W_{rec} increases with ΔP [25,26]. However, some of the stored energy in dielectrics will be dissipated during the depolarization/discharge process, which will be equal to the area of the *P-E* loop (i.e., W_{loss} can be seen in Figure 3) [27,28]. Such energy loss causes heat generation, consequently deteriorating the capacitor's thermal stability and lifespan. The heat generation is attributed to the dielectric loss ($tan\delta$) and temperature rise (ΔT), as provided using the following equations:

$$w_h = \pi \varepsilon_0 \varepsilon_r E^2 tan\delta \quad (8)$$

$$\Delta T = \frac{fV_e}{hA} W_h \quad (9)$$

where f is the driving frequency, V_e is the effective volume to an applied electric field, h is the heat transfer coefficient, and A is the total surface area of a sample [27,28]. Therefore, a low $tan\delta$ and a large ΔP (i.e., low P_r and high P_{max}) are critical parameters for achieving high energy storage performance in ceramic capacitors.

2.3.3. Dielectric Breakdown Strength

The energy storage response of ceramic capacitors is also influenced by the E_b, as the W_{rec} is proportional to the E, as can be seen in Equation (6) [29]. The BDS is defined as the maximum electric field over which the electrical resistance of a dielectric significantly decreases. The E_b of these capacitors strongly depends on intrinsic (bandgap, grain size, phase, defect dipoles, material thickness, microstructure, and porosity) and extrinsic (working/environmental conditions and electrode configuration) properties [5,30–33]. Therefore, a dense microstructure is a critical factor for the fabrication of a high-quality ceramic capacitor to achieve greater capacitance under high electric fields. However, dielectric breakdown is caused by pores, cracks, interfaces, and compositional inhomogeneity [31,33,34]. The porosity in dielectrics affects the dielectric breakdown strength and can cause overheating and thermal stress, resulting in breakdowns at higher electric fields [31,33].

2.3.4. Discharge Time

The discharge time is another critical parameter for energy storage. The discharging speed of a ceramic capacitor is calculated in terms of the discharge time, represented by $\tau_{0.90}$. It is defined as the time required for a capacitor to discharge 90% of its stored energy. The discharge time is 0.15 µs at an infinite time, and it depends on the dielectric permittivity and thickness of the material, load resistance, and applied voltage [6]. The discharge time should be very short for pulsed power energy storage capacitor applications.

2.3.5. Reliability

Dielectric capacitors are interconnected with their embedded system and operating conditions, influenced by various factors such as temperature, frequency, and voltage fluctuations. Therefore, better reliability, often called high electric fatigue endurance, protects the physical integrity of pulsed power systems, particularly dielectric capacitors, during energy storage under harsh circumstances. The evaluation of the resistance to stimuli can be conducted through observing the distinct features of *P-E* loops under particular investigation conditions.

2.4. Categories of Dielectric Materials

Based on polarization versus the electric field response, dielectric materials are categorized into linear dielectrics (LDs) and nonlinear dielectrics (NLDs), such as ferroelectrics (FEs), anti-ferroelectrics (AFEs), and relaxor ferroelectrics (RFEs). Figure 4a–d show a schematic of the electric field-dependent polarization response and corresponding ferroelectric domain structures with dipole orientation for the LDs and NLDs. LDs display an almost linear polarization response via the application of an electric field, owing to the lack of permanent dipoles (Figure 4a). Ferroelectric materials display superior polarization responses even in the absence of an external electric field due to the presence of a net dipole moment. Therefore, they have a strong nonlinear relation with the applied electric field (Figure 4b). In AFE materials, the adjacent dipoles are oriented in antiparallel directions, resulting in zero net polarization. They show double hysteresis loops at higher electric fields caused by AFE to FE phase transitions (Figure 4c). In RFEs, the existence of polar nanoregions (PNRs)/nanodomains greatly reduces cooperative coupling between ferroelectric domains, which limits spontaneous polarization and, consequently, slim *P-E* loops (Figure 4d).

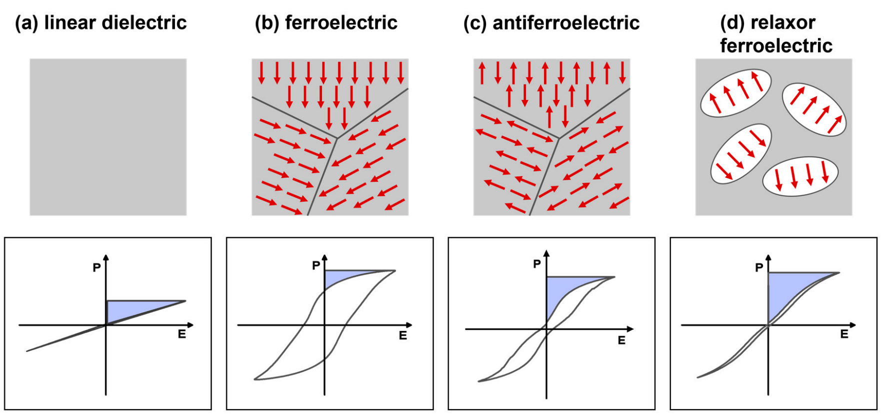

Figure 4. Schematic of the electric field-dependent polarization response and ferroelectric domain structures with dipole orientation for (**a**) LDs, (**b**) FEs, (**c**) AFEs, and (**d**) RFEs.

2.5. Energy-Storage Mechanism of the Materials

Ferroelectric materials are a fascinating class of dielectrics with unique properties, making them promising in the field of energy storage, conversion, and harvesting applications due to their electrical, mechanical, and thermal properties being intrinsically interrelated. All ferroelectrics are piezoelectric and pyroelectric materials, which make ferroelectrics extremely useful in multiple applications. The coupling of ferroelectric polarization to temperature, stress, and electric field enables various energy storage and conversion approaches that rely on diverse stimuli. The polarization is used in three ways, namely capacitive-energy storage (i.e., energy is stored in the form of polarization), piezoelectric-energy harvesting (i.e., vibration-induced stress on a piezoelectric material is converted into charge via a change in polarization), and pyroelectric-energy conversion (i.e., thermodynamic cycles can be utilized to convert temperature fluctuations into current) [35].

Based on the energy storage mechanism and the charge–discharge process, there is a substantial variation in the power density and energy density in dielectric capacitors, electrochemical capacitors, and batteries (see Figure 1b). Batteries offer higher energy density, but lower power density because of the slow movement of charges, which are used for long-term, stable energy supplies and applications with a maximum of 5 V [2,3,12,36]. Electrochemical capacitors have moderate power density and energy storage density with a slow charge–discharge rate and a low operating voltage (<3 V) [36]. Dielectric capacitors have high power density but limited energy storage density, with a more rapid energy transfer than electrochemical capacitors and batteries; this is because they store energy via dielectric polarization in response to the external electrical fields rather than chemical reactions [3,12,13,35]. Therefore, dielectric capacitors have received great interest due to their low price and high operating voltages (kV/MV range) for longer durations, making them ideal for a wide range of applications, including consumer electronics and advanced pulsed power devices.

3. Dielectric Materials for Energy Storage

3.1. Bulk Ceramics

3.1.1. Linear Dielectrics

LDs exhibit low energy loss, low relative dielectric permittivity, and a high breakdown electric field, and are promising for energy storage device applications under certain working conditions. Various LDs, such as Al_2O_3 [37], TiO_2 [38], $SrTiO_3$ (ST) [39–41], and $CaTiO_3$ (CT) [41–45], have been reported to improve their energy storage performances. Pure ST ceramics exhibited a relative dielectric permittivity of 300, a breakdown electric field of 1600 kV/mm, and a dielectric loss of 0.01 at RT, and are utilized for integrated circuit applications [39,42,46]. Chemical modifications have been adopted to enhance the energy storage properties in ST ceramic capacitors. Notably, 2 mol% of Ca doping in the ST system was improved energy density of 1.95 J/cm^3 and an efficiency of 72.3% at a breakdown field of 333 kV/cm, which is nearly three times higher than pure ST [41]. These improved energy storage properties in titanium-based ceramics are attributed to the insulation attenuation property caused by electronic hopping from the valence band to the conduction band. The substitution of Zr ions at the Ti site of $Sr_{0.98}Ca_{0.02}TiO_3$ boosted the energy storage density to 2.77 J/cm^3 and yielded an efficiency of 77.7% by reducing the dielectric loss and leakage current density, which is attributable to the higher chemical durability [47]. Mg-doped ST ceramics showed an enhanced W_{rec} of 1.86 J/cm^3 and η of 72.3% at a BDS of 362 kV/cm by lowering the dielectric loss to 0.001 with a moderate dielectric constant of 280 [45]. Interestingly, a binary composite of $CaZrO_3$-0.05$SrTiO_3$ exhibited a high W_{rec} of 5 J/cm^3 at 1000 kV/cm, caused by a low dielectric loss of 0.001 and dielectric constant of 35 [48]. It is well known that the BDS is directly proportional to the bandgap energy, and a higher bandgap energy enables a higher BDS [43,48]. Shay et al. [43] reported a binary composition of 0.8$CaTiO_3$-0.2$CaHfO_3$ (with 0.5 mol% of Mn doping) by modulating their bandgap energies, and showed a high W_{rec} of 9 J/cm^3 at 1200 kV/cm

(9.6 J/cm^3 at 1300 kV/cm). In a similar vein, BaZrO3-$CaTiO_3$ and $SrZrO_3$-$CaTiO_3$ binary compositions have shown improved energy storage performance [43,48].

3.1.2. Ferroelectrics

In comparison with LDs, FE materials show strong nonlinear behavior with high polarization, high dielectric permittivity, high energy loss, and a low BDS. Various rare earth elements and dopants (such as Sr, Ca, Nd, Mn, and Zr) were substituted at A/B-sites of the BT system to enhance the BDS and energy storage responses. Sr-doped BT ($Ba_{1-x}Sr_xTiO_3$, BST) ceramics were investigated, showing a high dielectric constant of 650, a low dielectric loss of 7.6×10^{-4} @ 1kHz, a low W_{rec} of 0.23 J/cm^3, and the Curie temperature being lowered far below RT [49]. Choi et al. [50] reported a defect dipole engineering method to enhance the energy storage performance by co-doping Nd and Mn in $Ba_{0.7}Sr_{0.3}TiO_3$ ceramics. Figure 5 presents a schematic illustration of a defect dipole concept between acceptor ions and oxygen vacancies in $Ba_{0.7}Sr_{0.3}TiO_3$ ceramics. These defect dipoles with a uniform and small-grained microstructure enable a high difference between P_{max} and P_r (ΔP~10.39 μC/cm^2) and capture electrons, improving the BDS to 110.6 kV/cm with co-doping of Nd and Mn; this in turn leads to improvements in the W_{rec} to 0.41 J/cm^3 and a high η of 84.6% in $Ba_{0.7}Sr_{0.3}TiO_3$ ceramics. Interestingly, Dong et al. [33] reported 1.6 wt% ZnO doped in $Ba_{0.3}Sr_{0.7}TiO_3$ ceramics with an enhanced W_{rec} of 3.9 J/cm^3 at 40 kV/mm. Taking a theoretical approach, Wang et al. [51] reported first-principles calculations and molecular dynamic simulations to study the effects of the chemical composition, phase under temperature, and electric fields on the ferroelectric and energy storage properties of ABO_3 perovskite FEs. These simulation results revealed a W_{rec} of 2.8 J/cm^3 and a η of 95% at E_b of 350 kV/cm in $Ba_{0.6}Sr_{0.4}TiO_3$ ceramics, and, furthermore, a W_{rec} of 30 J/cm^3 and a η of 92% obtained at an E_b of 2750 kV/cm in the same composition of $Ba_{0.6}Sr_{0.4}TiO_3$. However, practically, a BDS on the order of a thousand kV/cm is not achievable in most FEs because of numerous defects, an internal mechanical field, internal stress, and the influence of crystallographic lattice constants, phase transition, and grain size. Song et al. [52] reported the effect of grain sizes from 0.5 μm to 5.6 μm in $Ba_{0.6}Sr_{0.4}TiO_3$ ceramics to investigate the energy storage performance, and the samples with a grain size of 0.5 μm showed a high W_{rec} of 1.28 J/cm^3 at an E_b of 243 kV/cm.

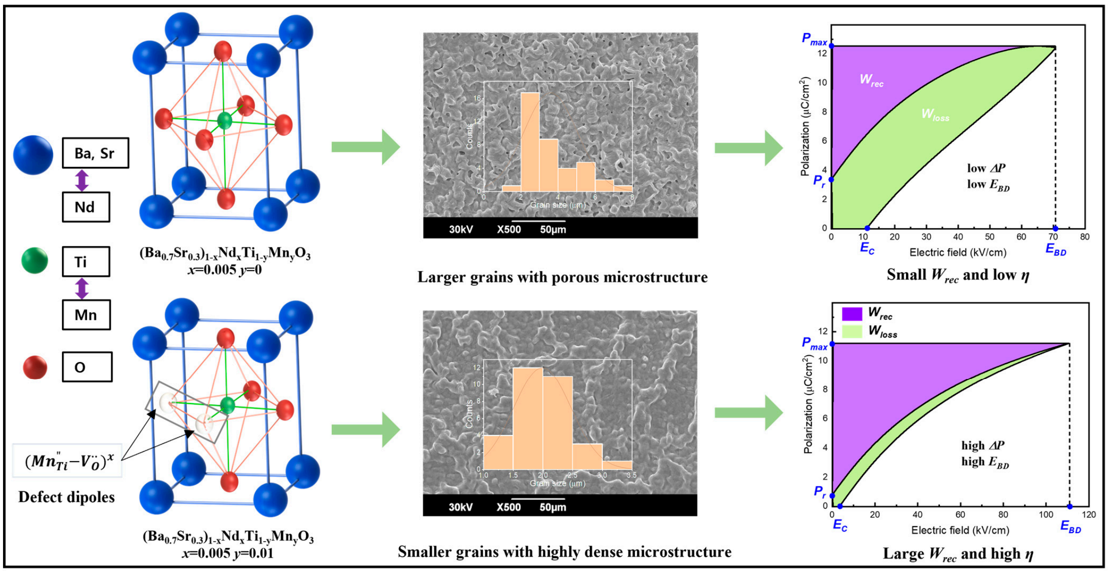

Figure 5. Schematic illustration of a defect dipole concept to achieve energy storage properties of Nd and Mn-co-doped $Ba_{0.7}Sr_{0.3}TiO_3$ ceramics. Defect dipoles between donor/acceptor ions and oxygen vacancies capture electrons, decrease grain size, and enable a high difference between P_{max} and P_r, thereby enhancing the BDS with Nd and Mn, which results in an improved W_{rec} and η in $Ba_{0.7}Sr_{0.3}TiO_3$ ceramics. Reproduced with permission [50]. Copyright 2023, MDPI.

3.1.3. Anti-Ferroelectrics

Antiferroelectric materials differ from typical ferroelectrics in their distinctive crystal structure, with adjacent diploes aligned in opposite orientations. To generate a strong ferroelectric state, diploes are subjected to a high electric field in order to realign their polarization orientation. This results in the formation of double hysteresis loops which consist of a linear polarization response in the AFE state and a ferroelectric hysteresis loop in the FE state. The huge reversible polarization would increase the energy storage density. However, thermal runaway and high energy dissipation due to hysteresis remain major challenges in building high energy density AFEs. To improve energy storage properties, enhancing the linear polarization response area and decreasing hysteresis loss by changing the phase transition parameters is recommended.

$PbZrO_3$ (PZ) AFE materials have been widely investigated due to their diverse phase transition features [53]. Chemical substitution affects reform polarization properties by altering the switching electric field between the AFE and FE phases. As per the phase diagram of La_2O_3-$PbZrO_3$-$PbTiO_3$ [54], Peixin et al. [55] reported the energy storage properties with the substitution of Ti^{4+} with Zr^{4+} at the B-site of in $(Pb_{1-y}La_y)(Zr_xTi_{1-x})O_3$ (PLZT) ceramics. The substitution of Zr^{4+} at Ti^{4+} can decrease the tolerance factor and improve the AFE properties. The *P-E* loops of PLZT AFEs become very slim with the substitution of the Zr concentration, and a high W_{rec} of 3.38 J/cm^3 and a high η of 86.5% were achieved with the optimized composition of x = 0.9 and y = 0.07 (Figure 6). Similarly, the substitution of La^{3+} at Pb^{2+} (the A-site) of $(Pb_{1-1.5x}La_x)(Zr_{0.5}Sn_{0.43}Ti_{0.07})O_3$ improved the AFE phase stability and provided slim P-E loops, resulting in the highest W_{rec} of 4.2 J/cm^3 and a high η of 78% for the x = 0.03 composition [56]. On the basis of the phase diagram of $PbZrO_3$-$PbTiO_3$-$PbSnO_3$ [57], Wang et al. [58] reported field-induced multiphase transitions (AFE-FE and FE-FE) at weak and high electric fields in $(Pb_{0.98}La_{0.02})(Zr_{0.55}Sn_{0.45})_{0.995}O_3$ AFE ceramics, yielding superior energy storage properties of a W_{rec} of 10.4 J/cm^3 and a η of 87% at 400 kV/cm. Moreover, Liu et al. reported the substitution of Sr^{2+} in $(Pb_{0.98-x}La_{0.02}Sr_x)(Zr_{0.9}Sn_{0.1})_{0.995}O_3$ AFE ceramics to improve the BDS and the switching of electric fields between the AFE and FE phase, resulting in an ultrahigh W_{rec} of 11.18 J/cm^3 and a high η of 82.2% [59].

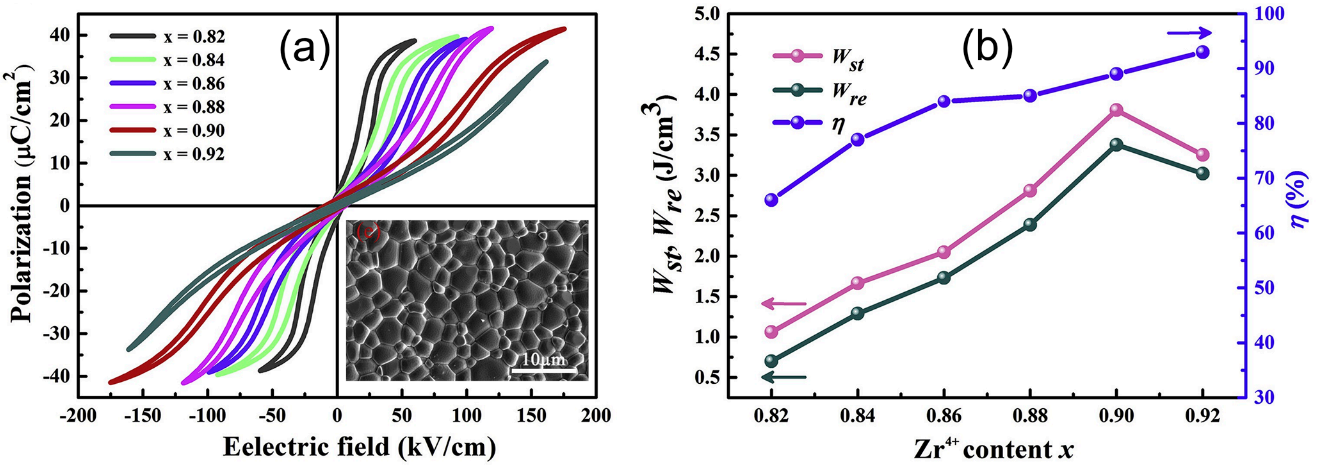

Figure 6. (**a**) P-E loops and (**b**) W_{st}, W_{re}, and η of the $(Pb_{1-y}La_y)(Zr_xTi_{1-x})O_3$ ceramics for y = 0.07 and x = 0.82 to 0.92. (**c**) shows a SEM image for x = 0.9. Reproduced with permission [55]. Copyright 2019, Elsevier.

In spite of the excellent features of AFE lead-based ceramics, various AFE lead-free ceramics have garnered attention due to environmental concerns. Zhao et al. [26] reported lead-free AFE $AgNbO_3$ (AN) ceramics with a Ta substitution to improve their energy storage properties. Figure 7 presents the *P-E* loops of pure, Ta-doped AN ceramics and energy storage properties of $Ag(Nb_{1-x}Ta_x)O_3$ ceramics as a function of the Ta concentration

(x = 0 to 20 mol%). A high W_{rec} of 4.2 J/cm^3 (260% higher than that of pure AN) and a η of 69% were achieved in $Ag(Nb_{1-x}Ta_x)O_3$ ceramics for x = 0.15. The substitution of Ta into the Nb site improves antiferroelectricity due to the lower polarizability of B-site cations, and also reduces grain size and enhances density, resulting in a high BDS of 240 kV/cm (Figure 7c). Researchers recently investigated the underlying mechanism between AFE properties and the energy barrier (EB), where increased and decreased EB for the AFE-FE phase transition via the doping of Sm^{3+}, Ca^{2+}, and the co-doping of Sm^{3+}/Ta^{5+} at the A- and A/B-sites of AN-based ceramics, which exhibited high W_{recs} of 5.2, 4.87, and 3.55 J/cm^3, respectively [60–62]. Luo et al. [63] reported a high W_{rec} of 6.3 J/cm^3 and a high η of 90%, realized by the M_2-M_3 phase boundary, the stabilized AFE phase, the presence of relaxor properties, and slim double *P-E* loops. In a similar way, Li et al. [5] reported $0.55(Bi_{0.5}Na_{0.5})TiO_3$-$0.45(Bi_{0.2}Sr_{0.7})TiO_3$ relaxor-antiferroelectric ceramics with a W_{rec} of 2.5 J/cm^3 for bulk ceramics and 9.5 J/cm^3 for multilayer ceramic capacitors, respectively. In addition, Qi et al. [64,65] fabricated $0.78(Bi_{0.5}Na_{0.5})TiO_3$-$0.22NaNbO_3$ and $0.76NaNbO_3$–$0.24(Bi_{0.5}Na_{0.5})TiO_3$ relaxor-antiferroelectric ceramics with giant energy storage properties as follows: a W_{rec} of 7.02 and 12.2 J/cm^3 and a η of 85% and 69%, respectively. Instead of the chemical substitution/composition method, Wang et al. [66] utilized a hydrothermal method to enhance the energy storage performance of AN ceramics and form a fine-grain size of 3 µm, which resulted in a high BDS of 250 kV/cm.

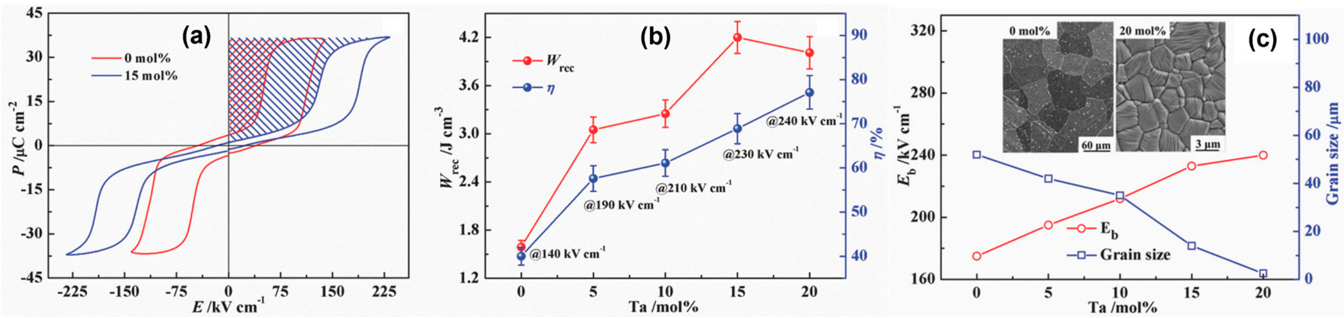

Figure 7. (**a**) *P-E* loops of $Ag(Nb_{1-x}Ta_x)O_3$ ceramics for x = 0 and 0.15, (**b**) W_{re} and η, and (**c**) E_b and grain size of $Ag(Nb_{1-x}Ta_x)O_3$ ceramics for x = 0 to 20. The inset of Figure 7c shows SEM images of $Ag(Nb_{1-x}Ta_x)O_3$ ceramics for x = 0 and 0.20. Reproduced with permission [26]. Copyright 2017, Wiley-VCH.

3.1.4. Relaxor Ferroelectrics

Relaxor ferroelectric materials, a significant subclass of ferroelectric materials, have drawn the attention of researchers because of their intriguing and little-known physics since Smolenskii's first discovery of the relaxor properties in a $BaTiO_3$ (BT)-based system [67]. The RFEs are thought to be the most promising energy storage materials for applications in electrostatic energy storage because of their distinct and slim P-E loops, in contrast with regular ferroelectrics, and are beneficial for energy storage. It has been established that the vast differences between RFEs and FEs are closely related to the dynamics of their domain structure. The nanodomains/PNRs, which range in size from several nm to µm and are more responsive to external electric fields, are predicted to facilitate a moderate P and slight P_r in RFEs, and these features are expected to contribute to a high W_{rec} and η [68]. In this regard, various lead-based and lead-free perovskite RFEs, namely $(Pb(Zn_{1/3}Nb_{2/3})O_3$-$PbTiO_3$ (PZN-PT) [69,70], $Pb(Mg_{1/3}Nb_{2/3})$ O_3-$PbTiO_3$ (PMN-PT) [70], (Pb, La)(Zr, Ti)O_3 (PLZT) [71] and BT [72–74], (Na, K)NbO_3 (KNN) [75,76], and (Bi, Na)TiO_3 (BNT) [75,76], have been explored for energy storage applications, respectively.

In lead-based RFEs, the PLZT has received strong attention for energy storage applications because of their phase structure (paraelectric phase, rhombohedral FEs, tetragonal FEs, orthorhombic AFEs, and RFEs) through chemical composition design. It is observed that relaxor properties showing slim P-E loops can be obtained via the formation of a pseudocubic structure with a c/a ratio approaching one when exceeding 7 mol% of La^{3+}

ions [77]. Thick/thin films have been fabricated to improve the BDS of the PLZT system. Hao et al. fabricated PLZT bulk ceramics with a thickness of 1 mm using a sol–gel synthesis process and an enhanced W_{rec} of 28.7 J/cm^3 and a η of 60% with a La:Zr:Ti ratio of 9:65:35 [78]. Furthermore, a Mn-doped PLZT thick film with the same ratio and same thickness showed a high W_{rec} of 30.8 J/cm^3 and a η of 68.4% at an electric field of 1185 kV/cm [79,80]. To date, the energy storage properties of PLZT with other lead-based RFEs and various chemical compositions have been reported, such as PZN-PT, PMN-PT, and Pb(Sn,Ti)O_3 (PST), exhibiting W_{rec} values ranging from 1 to 50 J/cm^3 for energy storage device applications [81–85]. However, the utilization of lead-based dielectrics has a strong impact on human health and the environment due to their toxicity. Thus, researchers have been developing lead-free RFEs for energy storage applications.

Over the past 20 years, since dielectric constant/polarization is independent of the applied electric field, temperature, and frequency, lead-free BT-based and weakly coupled RFEs have been explored in efforts to achieve high energy density and high efficiency based on the domain tailoring concept [4,23,86–94]. Ogihara et al. [86] reported a high W_{rec} of 6.1 J/cm^3 at 73 kV/mm in BT-BiScO_3 thick films that were sustained until 300 °C. Yuan et al. [93] reported a domain evaluation using chemical composition and improvements in the energy storage of BT-based ceramics. Furthermore, lead-free BNT-based and strongly coupled RFEs with a high polarization response via minimizing hysteresis loss and leakage currents have been reported. Qiao et al. [95] demonstrated a high W_{rec} of 4.14 J/cm^3 in a Sr and La-co-doped BNT system. The enhanced W_{rec} is attributed to the small grains and delays in polarization produced by La doping, whereas remnant polarization is decreased following Sr doping. Zhai et al. [96,97] utilized an A-site defect engineering method (nonstoichiometric ratio of Bi and Na) to reduce the electric conductivity and enhance the grain size, which resulted in a high W_{rec} (5.63 J/cm^3 and 3.72 J/cm^3) and a high η (94% and 90.7%) in binary and ternary systems, such as 0.75$Bi_{0.58}Na_{0.42}TiO_3$-0.25$SrTiO_3$ and BNT-$Bi_{0.1}Sr_{0.85}TiO_3$-$KNbO_3$. Wu et al. [98] reported the incorporation of $Sr_{0.85}Bi_{0.1\square 0.05}TiO_3$ (SBT) and $NaNbO_3$ (NN) into a BNT system via a compositional design. The substitution of Sr^{2+} ions and A-site vacancies constructed RFEs on the basis of the order–disorder theory, enabling a high W_{rec} of 3.08 J/cm^3 and a high η of 81.4%. Liu et al. [99] presented an intrinsic defect and polarization mechanism in A-site-deficient 0.66$(Bi_{0.5}Na_{0.5})TiO_3$-0.06$BaTiO_3$-0.28$(Bi_xSr_{1-3x/2})TiO_3$ (BNT-BT-BST) relaxors, favoring polarization behavior, which resulted in a W_{rec} of 1.61 J/cm^3 and a η of 90.5%. Hwang et al. [100] demonstrated the electric energy storage density and energy efficiency of $(1-x)Bi_{0.5}(Na_{0.8}K_{0.2})_{0.5}TiO_3$-$xBi_{0.2}Sr_{0.7}TiO_3$ (BNKT-BST; x = 0.15–0.50) RFEs via a domain engineering method. The substitution of BST composition into the BNKT system can disturb the long-range ferroelectric order, reducing the dielectric maximum temperature T_m, which leads to the formation of dynamic PNRs (Figure 8a). Additionally, the T_m was shifted to a higher temperature with increasing frequency, signifying RFE behavior in BNKT-BST ceramics, which is supported by the modified Curie Weiss law (Figure 8b). The relaxor properties contribute to a higher P_{max} and a lower P_r, enhancing the BDS with the incorporation of BST, and leading to a high W_{rec} of 0.81 J/cm^3 and high η of 86.95% at an electric field of 90 kV/cm for a x = 0.45 composition (Figure 8c,d). Ma et al. [101] utilized a morphotropic phase boundary (MPB) 0.76$Bi_{0.5}Na_{0.5}TiO_3$-0.24$SrTiO_3$ (BNT-ST) RFE with the incorporation of AFE AN to a lower P_r and retained the same P_{max} in order to achieve a W_{rec} of 2.03 J/cm^3. Furthermore, lead-free KNaNbO3-based RFEs have been explored to enhance their energy storage properties. Yang et al. [102] reported composition-driven grain size to a sub-micrometer scale (~100–200 nm) to enhance the breakdown strength of $(K_{0.5}Na_{0.5})NbO_{3-}xSrTiO_3$ (KNN-ST) RFEs, and showed a high W_{rec} of 4.03 J/cm^3 at 400 kV/cm. Similarly, KNN has been modified with $BiFeO_3$, $Sr(Sc_{0.5}Nb_{0.5})O_3$, and $Bi(Mg_{2/3}Nb_{1/3})O_3$ ceramics, and high W_{rec} values of 2 J/cm^3, 2.60 J/cm^3, and 4.08 J/cm^3 were achieved [34,65,103,104]. Xie et al. [105] reported an ultra-high W_{rec} of 8.73 J/cm^3 and a high η of 80.1% in 0.68 $NaNbO_3$-0.32$Bi_{0.5}Li_{0.5}TiO_3$ ceramics, achieved via exploiting the stable orthorhombic FE phase instead of the AFE orthorhombic phase (Figure 9a,b). In addition, they introduced the AFE relaxor concept to discuss the energy storage performance of 0.78NN-0.24BNT systems. They reported that the local AFE was transformed/reversed into the FE phase at an electric field of 400 kV/cm, inducing a large P_{max} (50 μC/cm^2) and a low P_r of 5 μC/cm^2, which together provided an enhanced ultra-high W_{rec} of 12.2 J/cm^3 and a high η of 69% at an electric field of 680 kV/cm, as shown in Figure 9c,d [65]. The energy storage properties of ceramic-based dielectric materials are listed in Table 1.

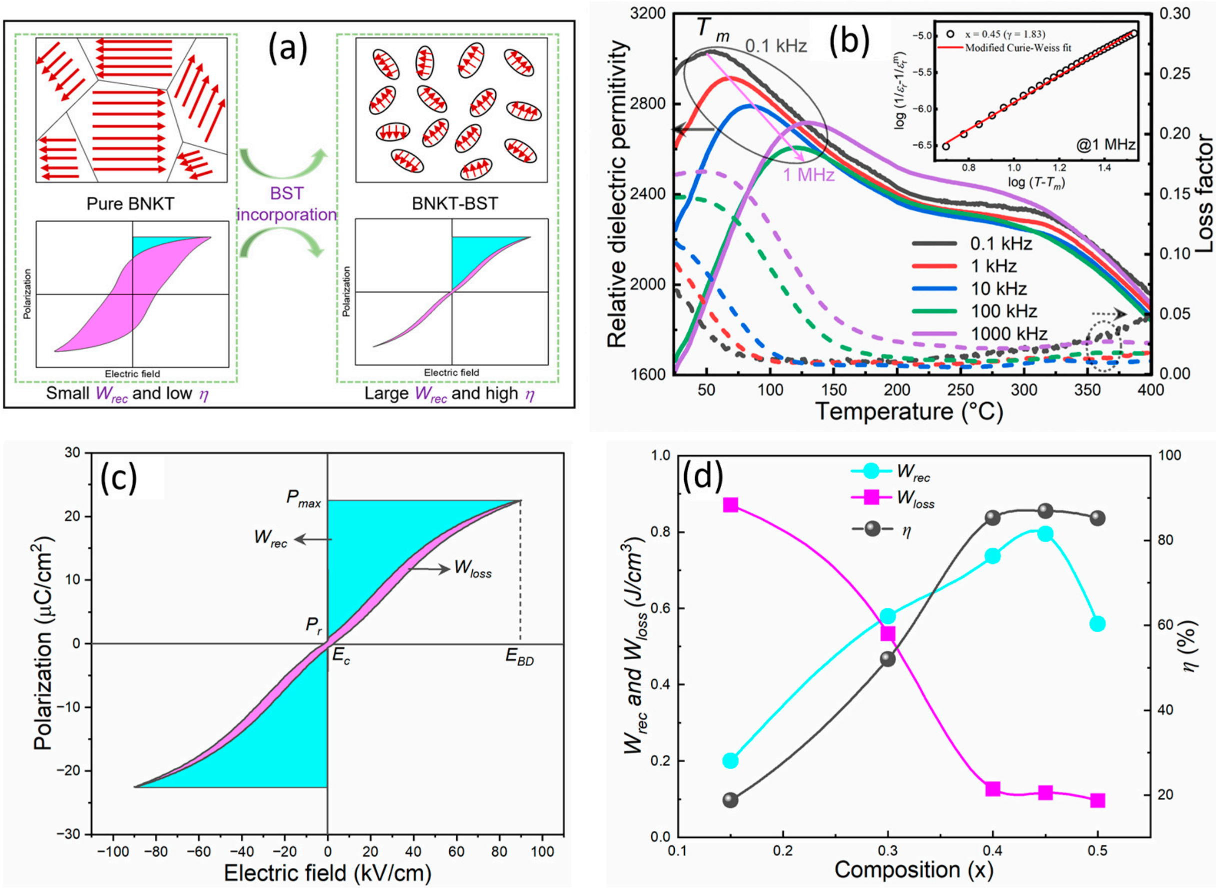

Figure 8. (**a**) Schematic of the domain structure and formation of the FE to RFE transition with the incorporation of BST into BNKT, leading to improved W_{rec} and η (where the red arrows indicate the dipole orientation). (**b**) Temperature dependence of the relative dielectric permittivity and loss factor of 0.55BNKT-0.45BST composition. The inset of Figure 8b presents the $log(T - T_m)$ versus $log\left[\left(\frac{1}{\varepsilon_r}\right) - \left(\frac{1}{\varepsilon_r^m}\right)\right]$ of 0.55BNKT-0.45BST at 1 MHz. (**c**) *P-E* hysteresis loop of 0.55BNKT-0.45BST ceramics. (**d**) Composition versus W_{rec}, W_{loss}, and η for x = 0.15–0.50. Reproduced with permission [100]. Copyright 2023 MDPI.

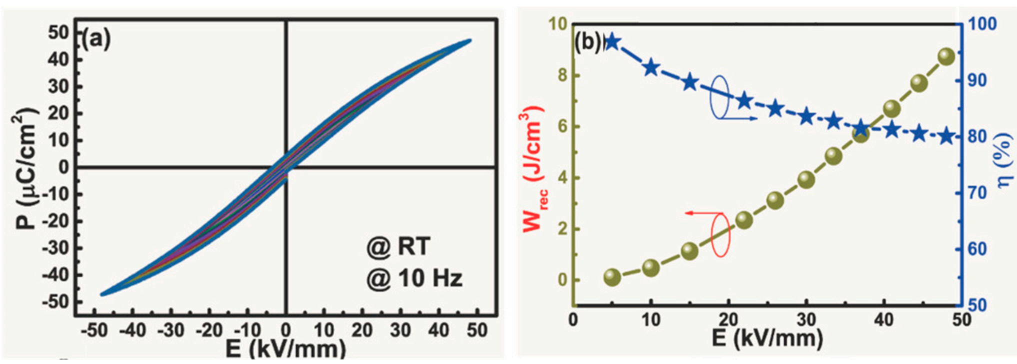

Figure 9. *Cont.*

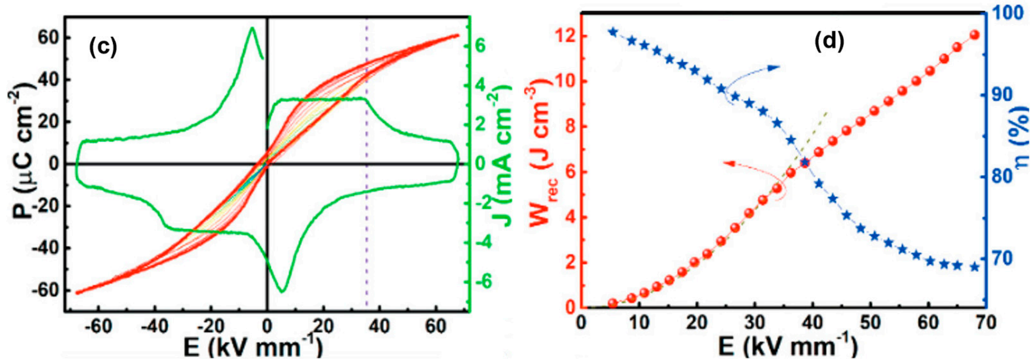

Figure 9. (**a**) *P-E* loops and (**b**) W_{rec} and η values of 0.68 NN-0.32BLT ceramics at various fields. (**c**) P−E loops along with the current density versus electric field curve. Reproduced with permission [105]. Copyright 2021 John Wiley and Sons. (**d**) W_{rec} and η values of 0.76 NN-0.24BNT ceramics at various fields and measured at 10 Hz and RT. Reproduced with permission [65]. Copyright 2019 John Wiley and Sons.

Table 1. Energy storage properties of ceramic-based dielectric bulk materials.

Bulk Ceramics	Composition	W_{rec} (J/cm^3)	η (%)	E_b (kV/cm)	Refs.
	$Ca_{0.5}Sr_{0.5}(Ta_{0.024}Ti_{0.97})O_3$-2 wt%$SiO_2$	2	96	360	[106]
LDs	$Ca_{0.5}Sr_{0.5}Ti_{0.97}Sn_{0.03}O_3$	2.06	95	330	[107]
	$Ca_{0.5}Sr_{0.5}Ti_{0.9}Zr_{0.1}O_3$	2.05	85	390	[108]
	$(Ca_{0.5}Sr_{0.5})_{0.8875}La_{0.075}TiO_3$	2.07	93	370	[109]
	$0.7(Bi_{0.5}K_{0.5}TiO_3)$-$0.3SrTiO_3$	2.31	77.7	190	[110]
	$(Ca_{0.5}Sr_{0.5})_{0.99}Mg_{0.01}TiO_3$	2.88	90	460	[111]
	$Ca_{0.5}Sr_{0.5}Ti_{0.85}Zr_{0.15}O_3$	3.37	96	440	[112]
	$0.9(Sr_{0.7}Bi_{0.2}TiO_3)$-$0.1Bi(Ni_{2/3}Nb_{1/3})O_3$	3.71	97	340	[113]
	Ca-doped $SrTiO_3$	1.95	72.3	333	[41]
	Zr doped $Sr_{0.98}Ca_{0.02}TiO_3$	2.77	77.7	-	[47]
	Mg-doped $SrTiO_3$	1.86	72.3	362	[45]
	$CaZrO_3$-$0.05SrTiO_3$	5	-	1000	[48]
	$0.8CaTiO_3$-$0.2CaHfO_3$	9	-	1200	[43]
FEs	$Ba_{0.3}Sr_{0.7}TiO_3$	0.23	95.7	90	[49]
	Nd and Mn-doped $Ba_{0.7}Sr_{0.3}TiO_3$	0.41	84.6	110.6	[50]
	1.6 wt% ZnO doped $Ba_{0.3}Sr_{0.7}TiO_3$	3.9	-	40	[33]
	$(BaCa)(ZrTi)O_3$	1.28	-	243	[52]
	$BiFeO_3$–$BaTiO_3$–$Bi(Mg_{2/3}Nb_{1/3})O_3$	1.27	-	110	[114]
	$BaTiO_3$–$Bi(Zn_{2/3}(Nb_{0.85}Ta_{0.15})_{1/3})O_3$	2.06	78	180	[115]
	$0.9BaTiO_3$-$0.1Bi(Mg_{1/2}Hf_{1/2})O_3$	3.38	87	240	[116]
AFEs	$(Pb_{0.91}Ba_{0.045}La_{0.03})(Zr_{0.6}Sn_{0.4})O_3$	8.16	92.1	340	[117]
	$0.84(Bi_{0.5}Na_{0.5})TiO_3$-$0.16KNbO_3$	5.2	88	310	[118]
	$Ag_{0.76}La_{0.08}NbO_3$	7.01	77	476	[119]
	$Ag_{0.97}Nd_{0.01}Ta_{0.20}Nb_{0.80}O_3$	6.5	71	370	[120]
	$NaNbO_3$-$Bi(Zn_{2/3}Nb_{1/3})O_3$	2.4	90	300	[121]
	$0.85(NaNbO_3)$-$0.15(Bi(Ni_{2/3}Nb_{1/3})O_3)$	3.31	80.9	440	[122]

Table 1. *Cont.*

Bulk Ceramics	Composition	W_{rec} (J/cm^3)	η (%)	E_b (kV/cm)	Refs.
AFEs	$(Na_{0.41}La_{0.09})(Nb_{0.82}Ti_{0.18})O_3$	6.5	66	550	[123]
	$0.75[0.90NaNbO_3$-$0.10Bi(Mg_{0.5}Ta_{0.5})O_3]0.25(Bi_{0.5}Na_{0.5})_{0.7}Sr_{0.3}TiO_3$	8	90.4	800	[124]
	$0.68NaNbO_3$-$0.32(Bi_{0.5}Li_{0.5})TiO_3$	8.73	80.1	-	[105]
	$0.76NaNbO_3$-$0.24(Bi_{0.5}Na_{0.5})TiO_3$	12.2	69	680	[65]
RFEs	$0.93BaTiO_3$-$0.07YNbO_4$	0.61	87	173	[125]
	$0.65Bi1_{.05}FeO_3$-$0.35BaTiO_3$-$(BiNa_{0.84}K_{0.16})_{0.48}Sr_{0.04}TiO_3$	0.81	60	100	[126]
	$0.93BaTiO_3$-$0.07Sr(Zn_{1/3}Nb_{2/3})O_3$	1.45	83.12	260	[127]
	$0.88BaTiO_3$-$0.12Bi(Ni_{2/3}Nb_{1/3})O_3$	2.09	95.9	220	[128]
	0.02Ce-doped $0.65BaTiO_3$-$0.35Sr_{0.7}Bi_{0.2}TiO_3$	2.57	81.3	330	[129]
	$(Ba_{0.65}Sr_{0.24}5Bi_{0.07})_{0.99}Nd_{0.01}TiO_3$	4.2	80	460	[130]
	$0.85(0.95Bi_{0.5}Na_{0.5}TiO_3$-$0.05SrZrO_3)$-$0.15NaNbO_3$	3.14	79	230	[131]
	$Na_{0.25}Bi_{0.2}5Sr_{0.5})(Ti_{0.8}Sn_{0.2})O_3$	3.4	90	310	[132]
	$0.88Bi_{0.47}Na_{0.47}Ba_{0.06}TiO_3$-$0.12CaHfO_3$	4.2	66.7	280	[133]
	$0.75(Bi_{0.45}La_{0.05}Na_{0.5})_{0.94}Ba_{0.06}TiO_3$-$0.25Sr_{0.8}Bi_{0.1}\square_{0.1}Ti_{0.8}Zr_{0.2}O_{2.95}$	3.84	90.8	330	[134]
	$0.5(Na_{0.5}Bi_{0.5}TiO_3)$-$0.5(Sr_{0.85}Sm_{0.1}TiO_3)$	5.02	90	422	[135]
	$0.8Bi_{0.5}Na_{0.5}TiO_3$-$0.2SrNb_{0.5}Al_{0.5}O_3$	6.64	96.5	520	[136]
	$0.70Bi_{0.5}Na_{0.5}TiO_3$-$0.30SrNb_{0.5}Al_{0.5}O_3$	6.78	89.7	572	[137]
	$0.85K_{0.5}Na_{0.5}NbO_3$-$0.15Bi(Li_{0.5}Ta_{0.5})O_3$	1.1	56	151	[138]
	$0.91K_{0.5}Na_{0.5}NbO_3$-$0.09SrZrO_3$	2.81	80	370	[139]
	$0.9(K_{0.5}Na_{0.5})NbO_3$-$0.1Bi(Zn_{2/3}Nb_{1/3})O_3$	4.01	97.1	326	[140]
	$[(Na_{0.5}K_{0.5})_{0.91}Li_{0.03}](Nb_{0.88}Sb_{0.06})O_3$-$0.06Bi(Zn_{1/2}Zr_{1/2})O_3$	4.85	88.2	480	[141]
	$0.85K_{0.5}Na_{0.5}NbO_3$-$0.15Bi(Zn_{2/3}Ta_{1/3})O_3$	6.7	92	600	[142]
	$0.90K_{0.5}Na_{0.5}NbO_3$-$0.10Bi(Zn_{2/3}(Nb_{0.85}Ta_{0.15})_{1/3})O_3$	7.4	78	800	[143]
	$0.85K_{0.5}Na_{0.5}NbO_3$-$0.15Bi(Ni_{0.5}Zr_{0.5})O_3$	8.09	88.46	870	[144]

3.2. Ceramic Films

In Section 3.1.4, we presented lead-free RFE materials, which are good candidates for energy storage device applications, owing to their ultra-high energy storage density, excellent BDS, and eco-friendliness. However, the miniaturization of electronic devices is necessary for real-world applications, such as hybrid electric vehicles, defense artillery, and smart and wearable electronics [145–147]. Therefore, thin/thick film capacitors (e.g., RFEs) have received significant attention in developing high-performance ceramic capacitors for energy storage as compared to bulk ceramic capacitors (LDs, FEs, and AFEs) [1,148–150]. Interestingly, these film capacitors have a higher BDS due to less defects, which results in a high energy density. In addition, thin/thick film capacitors are promising for miniaturized electronic devices due to their uniform and highly dense microstructure. The thickness of ceramic capacitors plays an important role in determining the BDS. The thickness/volume ratio of a film capacitor determines its energy storage capacity. Moreover, ceramic capacitor devices with a higher BDS are safe for operation at high voltages and have a smaller likelihood of device failure [6,151].

RFE film-based dielectric capacitors that adopt various strategies for energy storage have been investigated [152–169]. Zhang et al. [170] improved the energy storage performance via a small amount of Mn doping (1 mol.%) in 0.70BNT-0.3ST RFE thin films. Mn^{2+} ions induce an intrinsic restoring force and enable the reversible domain switching and slim *P-E* loops (ΔP~56 μC/cm^2), resulting in a high W_{rec} of 27 J/cm^3. The same amount of Mn in 0.6ST-0.4BNT thin films yielded a high W_{rec} of 33.58 J/cm^3 at a BDS of 3134 kV/cm, owing to reduced oxygen vacancies [171]. Interestingly, BNT-BT has shown excellent dielectric properties at the MPB between the coexistence of a rhombohedral FE phase and a tetragonal AFE phase for x = 0.06. Peng et al. [172] reported an ultra-high W_{rec} of 154 J/cm^3 via the co-doping of La and Zr in 0.94BNT-0.06BT RFE thin films. The La dopant plays a critical role in enhancing the relaxor properties, whereas the Zr dopant was utilized to control the transition temperature. Pan et al. [173] reported an energy density of 70 J/cm^3 in 0.55$BiFeO_3$–0.45$SrTiO_3$ (BF-ST) films via a domain engineering method. The substitution of ST into BF can transform the micrometer-scale FE domains into highly dynamic PNRs, resulting in a high energy storage density in the BF-ST films. In addition, they demonstrated that the coexistence of rhombohedral and tetragonal nanodomain structures in a cubic paraelectric matrix creates a flattened domain-switching pathway in BF-BT-ST films, which minimizes hysteresis loss and delivers an energy density of 112 J/cm^3 [152]. Pan and co-workers carried out phase-field simulations in order to choose the proper combination of BF and BT with Sm doping to achieve high energy storage. These simulations were helpful in designing super-paraelectric RFEs with unique and smaller size nanodomains in a Sm-doped BF-BT system, which generated an ultra-high W_{rec} of 152 J/cm^3 and a high η of 90% [174]. The energy storage properties of the ceramic films are summarized in Table 2.

Table 2. Energy storage properties of ceramic films.

Film Composition	W_{rec} (J/cm^3)	η (%)	E_b (kV/cm)	Refs.
$BiFeO_3$-$BaTiO_3$-$SrTiO_3$	112	80	5.3 × 10^3	[152]
0.5$Ba(Zr_{0.2}Ti_{0.8})O_3$–0.5$(Ba_{0.7}Ca_{0.3})TiO_3$ (BCZT)	99.8	71	750	[153]
0.6$(Bi_{0.5}Na_{0.5})TiO_3$–0.4$Bi(Ni_{0.5}Zr_{0.5})O_3$	50.1	63.9	2200	[154]
Mn-doped 0.97(0.93$Na_{0.5}Bi_{0.5}TiO_3$-0.07$BaTiO_3$)-0.03$BiFeO_3$	81.9	64.4	2285	[155]
Mn-doped 0.55(0.94$Na_{0.5}Bi_{0.5}TiO_3$-0.06$BaTiO_3$)-0.45$SrTiO_3$	76.1	80	2813	[156]
$Ba(Zr_{0.35}Ti_{0.65})O_3$	65.1	72.9	6.15 × 10^3	[157]
Sn-doped In_2O_3/$BaZr_{0.35}Ti_{0.65}O_3$	40.6	68.9	4.23 × 10^3	[158]
0.9$Bi_{0.2}Sr_{0.7}TiO_3$–0.1$BiFeO_3$	48.5	47.57	4800	[159]
Mn-doped $BiFeO_3$–$BaTiO_3$	80	78	3.1 × 10^3	[160]
0.5$(Bi_{0.5}Na_{0.5})TiO_3$-0.5$Bi(Zn_{0.5}Zr_{0.5})O_3$	40.8	64.1	1500	[161]
0.88$Ba_{0.55}Sr_{0.45}TiO_3$–0.12$BiMg_{2/3}Nb_{1/3}O_3$	86	73	5 × 10^3	[162]
0.3$Bi(Fe_{0.95}Mn_{0.05})O_3-0.7(Sr_{0.7}Bi_{0.2})TiO_3$	61	75	3000	[163]
$(Na_{0.8}K_{0.2})_{0.5}Bi_{0.5}TiO_3$/0.6$(Na_{0.8}K_{0.2})_{0.5}Bi_{0.5}TiO_3-0.4SrTiO_3$	73.7	68.1	2308	[164]
$Na_{0.5}Bi_{3.25}La_{1.25}Ti_4O_{15}$/$BaBi_{3.4}Pr_{0.6}Ti_4O_{15}$	159.7	70	3450	[165]
Mn-doped 0.65(0.94$Na_{0.5}Bi_{0.5}TiO_3$–0.06$BaTiO_3$)–0.35$SrTiO_3$	56	66	2738	[166]
$Sr_{0.975}(Bi_{0.5}Li_{0.5})_{0.025}Ti_{0.99}Mn_{0.01}O_3$	47.7	66.5	3307	[167]
$Ba(Zr_{0.1}Ti_{0.9})O_3$	15.5	69.8	1500	[168]
HfO_2/Al_2O_3/ZrO_2	54.3	51.3	5000	[169]

3.3. Multilayer Ceramic Capacitors

MLCCs have received extensive attention in the field of energy storage capacitor applications due to their ultra-high energy density, efficiency, and fast charge–discharge rates [175–179]. In recent years, the energy storage performance was improved in RFE $Bi_{0.5}Na_{0.5}TiO_3$ and AFE $AgNbO_3$-based lead-free ceramics, attaining energy densities of 2.7 J/cm^3 and 4.2 J/cm^3, respectively [26,177,178,180–186]. However, high energy dissipation and poor stability are attributed to the AFE to FE phase transition, which are the main drawbacks of AFEs limiting their practical applications. In this regard, Li et al. [5] demonstrated 0.55($Bi_{0.5}Na_{0.5}$)TiO_3 (BNT)-0.45($Bi_{0.2}Sr_{0.7}$)TiO_3 (BST) MLCCs and improved their energy density and efficiency by combining RFE and AFE features. The RFE exhibits highly dynamic polar nano-regions and disrupts the long-range ferroelectric order, which results in a hysteresis-free *P-E* loop. The RFE BST displaying a diffused phase transition was utilized with BNT to obtain RFE features, and is expected to reduce polarization and the high ΔP.

MLCCs have been fabricated using the tape-casting technique, which has two main advantages as follows: (i) The MLCC layers offer low porosity and a fine grain size, leading to a high E_b. (ii) A higher E_b is expected in the MLCC compared to conventional ceramic capacitors because the E_b increases with the decreasing layer thickness. The fabrication process of the MLCCs entails various stages, such as ball milling, slurry formation, tape casting, screen printing, stacking/lamination, dicing, sintering, and termination dipping. Figure 10 presents a schematic illustration of the MLCC fabrication process [187,188]. The ceramic powders were ball milled, slurry dried, and calcined. This calcined powder was re-milled with a dispersant (ethyl methyl ketone), binder (poly(propylene carbonate)), and plasticizer (butyl benzyl phthalate). Furthermore, a slurry was used to prepare thick films using a tape-casting process. The films were stacked layer by layer with inner printed Pt electrodes and then sintered at the desired temperatures to obtain the MLCCs. Lastly, the sintered samples were polished to terminate the opposite ends of the MLCC, and silver paste was coated to form the outer electrodes for electrical characterizations.

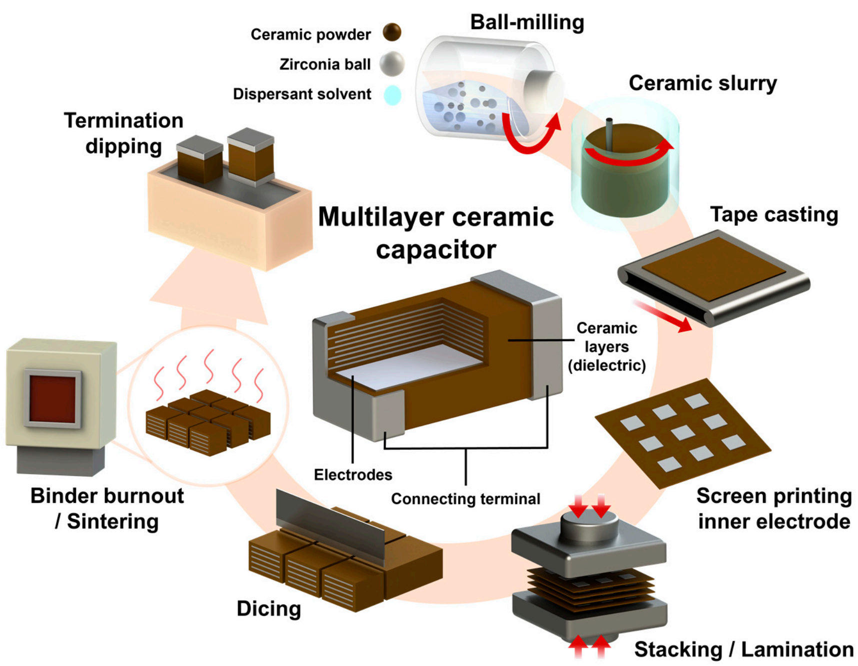

Figure 10. Schematic diagram of the MLCC fabrication process.

Figure 11a shows the unipolar polarization and current versus electric field curve for a 0.55($Bi_{0.5}Na_{0.5}$)TiO_3 (BNT)-0.45($Bi_{0.2}Sr_{0.7}$)TiO_3 (0.55BNT-0.45SBT) ceramic sample. It exhibited a high energy storage density of 2.5 J/cm^3 and a high efficiency of 95% at a high breakdown field of 20 MV/m. The temperature dependence of the relative dielectric permittivity and the loss factor of the 0.55BNT-0.45SBT sample are shown in Figure 11b. The dielectric maximum temperature (T_m) shifted towards higher temperatures, and the dielectric peaks diffused with increasing frequency, revealing the formation of high-dynamic polar nanoregions (PNRs); such materials are called relaxor ferroelectrics [189,190]. The degree of the diffuseness (γ) of the 0.55BNT-0.45SBT sample is found to be 1.85, indicating strong relaxor behavior (Figure 11c). Due to the formation of PNRs, the 0.55BNT-0.45SBT ceramic sample exhibits a high relative dielectric permittivity, high energy density, and high energy efficiency. To achieve ultrahigh energy density, 0.55BNT-0.45SBT MLCCs were fabricated using the tape-casting method. They consist of 10 dielectric layers with a total thickness of 200 μm and an inner electrode area of 6.25 mm^2 (each layer has a thickness of 20 μm), as shown in Figure 11d. The surface morphology of the MLCC is shown in Figure 11e. The breakdown electric field was increased to 72 MV/m due to the advantages of the MLCCs fabricated using the tape-casting method, which offers low porosity and a fine grain size when compared to their counterpart bulk ceramics [191]. In general, the breakdown strength of the ceramics increases as the layer thickness decreases, as observed in many ceramics [192,193]. Figure 11f shows the energy density and efficiency as a function of the electric field for 0.55NBT-0.45SBT MLCCs. The energy storage density of these MLCCs exhibited a high W_{rec} of 9.5 J/cm^3 and a η of 92% at 72 MV/m. These results indicate that combining the antiferroelectric and relaxor properties of MLCCs is a promising approach for improving the energy storage responses in order to meet the requirements of advanced energy storage devices. In recent years, various strategies, including controlled phase [177], chemical homogeneity [178], grain orientation [194], combining antiferroelectric and relaxor properties [5], heterovalent doping [195], and two-step sintering [196], etc., were adopted to enhance the energy storage performance of MLCCs, as summarized in Table 3. In general, as the layer thickness decreases, the BDS of solid dielectrics increases [197]. Thin films show a higher BDS when compared to bulk ceramics and MLCs due to the minimal thickness and less defects, but they have limitations in energy storage density and efficiency. MLCCs have a lower BDS than thin films, but they have other advantages, such as a compact size, a balance between the BDS and energy storage, and good temperature stability, which play an important role in practical applications, especially in pulsed power systems.

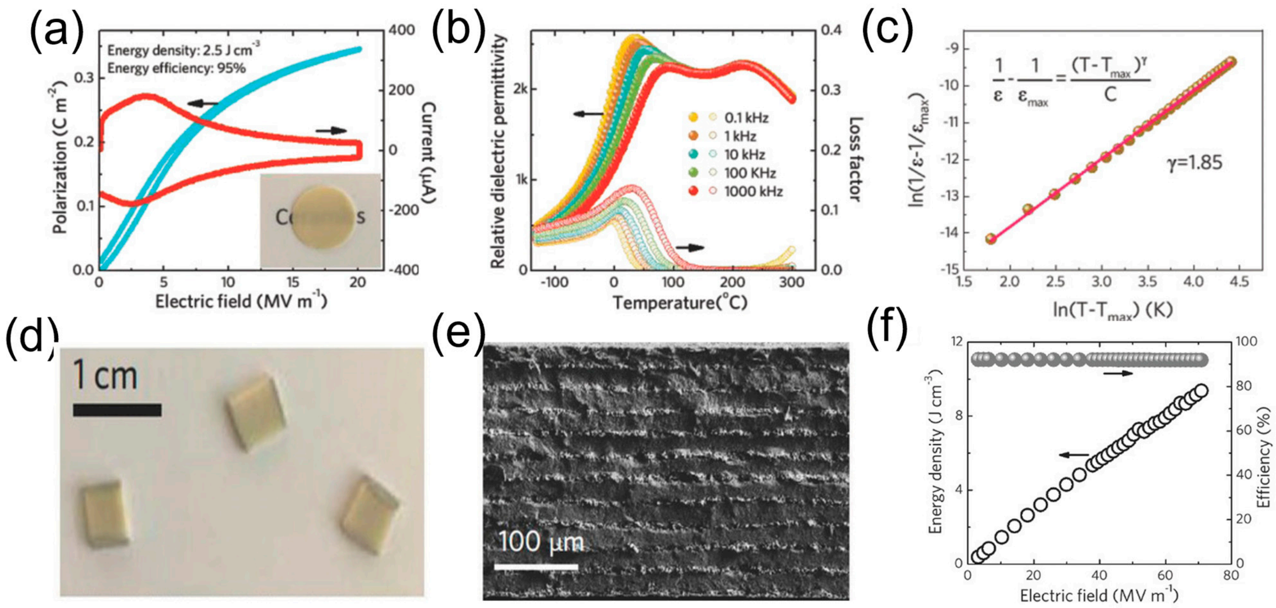

Figure 11. (**a**) Polarization (blue curve) and current (red curve) response are a function of the electric field (the inset shows a picture of the bulk sample), (**b**) the temperature variation of relative dielectric permittivity and loss factor, and (**c**) $ln(T-T_{max})$ versus $ln\left[\left(\frac{1}{\varepsilon}\right)-\left(\frac{1}{\varepsilon_{max}}\right)\right]$ of 0.55($Bi_{0.5}Na_{0.5}$)TiO_3-0.45($Bi_{0.2}Sr_{0.7}$)TiO_3 ceramics. (**d**,**e**) A photograph and SEM image of MLCC of 0.55($Bi_{0.5}Na_{0.5}$)TiO_3-0.45($Bi_{0.2}Sr_{0.7}$)TiO_3. (**f**) Energy density and efficiency versus the applied electric field of 0.55($Bi_{0.5}Na_{0.5}$)TiO_3-0.45($Bi_{0.2}Sr_{0.7}$)TiO_3 MLCC. Reproduced with permission [5]. Copyright 2018, Wiley-VCH.

Table 3. Energy storage properties of MLCCs.

MLCC Composition	Thickness/No. of Active Layers	W_{rec} (J/cm^3)	η (%)	E_b (kV/cm)	Refs.
$0.75(Bi_{1-x}Nd_x)FeO_3$-$0.25BaTiO_3$ (x = 15%)	32 µm/9	6.74	77	540	[177]
$0.87BaTiO_3$-$0.13Bi(Zn_{2/3}(Nb_{0.85}Ta_{0.15})_{1/3})O_3$	17 µm/10	8.13	95	750	[196]
$0.55(Bi_{0.5}Na_{0.5})TiO_3$-$0.45(Bi_{0.2}Sr_{0.7})TiO_3$	20 µm/10	9.5	92	720	[5]
0.62BF–0.3BT-$0.08NdZn_{0.5}Zr_{0.5}O_3$	16 µm/7	10.5	87	700	[178]
$Sm_{0.05}Ag_{0.85}Nb_{0.7}Ta_{0.3}O_3$	10 µm	14	85	1450	[195]
$0.5BiFeO_3$-$0.4SrTiO_3$-0.03Nb-0.1 $BiMg_{2/3}Nb_{1/3}O_3$	8 µm	15.8	75.2	1000	[198]
<111>$Na_{0.5}Bi_{0.5}TiO_3$-$Sr_{0.7}Bi_{0.2}TiO_3$	20 µm/10	21.5	65	103×10^3	[194]
$Ba_{0.3}Sr_{0.7}TiO_3$/$0.85BaTiO_3$-$0.15Bi(Mg_{0.5}Zr_{0.5})O_3$	230 nm/8	30.64	70.93	3000	[199]
$Ba_{0.7}Ca_{0.3}TiO_3$-$BaZr_{0.2}Ti_{0.8}O_3$	100 nm/8	52.4	72.3	4.5×10^3	[176]

4. Challenges and Future Prospects

With the discovery of new materials and strategies, the energy storage density of bulk ceramics, thin films, and MLCCs has been greatly improved to 12, 159, and 52 J/cm^3, respectively, as summarized in Tables 1–3. Even with the tremendous advancements, there are still certain challenges in real-world applications. Dielectric ceramics with a high energy storage density of more than 8 J/cm^3 with a high efficiency of over 90% are still scarce and cannot meet the demands of miniature advanced electronic and electric power systems. To achieve a high energy storage density in dielectrics, researchers mostly focused on the enhancement of ΔP and E_b. Extensively utilized strategies for enhancing E_b are reducing the grain size with homogeneous microstructures, stimulating electrical homogeneity, raising resistance, enhancing thermal conductivity, and lowering dielectric losses. These strategies can be implemented by employing advanced sintering procedures, adding sintering aids, employing two-step sintering, adjusting the heating/cooling rate/holding time, and making composite materials. However, effective strategies for further improving the E_b remain limited. To obtain a high ΔP, the most popular method is to choose a host material with strong ferroelectricity and then decrease its P_r via composition doping. On the other hand, select a host material with a modest P_r and then add a secondary compound to enhance its P_{max}. However, it remains challenging to achieve both a high P_{max} and a low P_r in these solid solutions. The domain engineering method allows for the fabrication of dielectrics with a low P_r and a moderate ΔP via producing PNRs/nanodomains. However, the P_{max} value remains low, restricting the raise of the W_{rec}. Recently introduced local region design techniques, such as designing local regions with polarization-field response behavior or constructing local regions with polymorphic PNRs via phase structure regulation, will be an excellent choice for developing dielectrics with a high P_{max} and a low P_r.

Developing dielectric materials with a high W_{rec} and η remains the path of future research. In addition, the trade-off between the W_{rec} and η and the contradiction between the ε_r and the E_b must be resolved. New materials, new manufacturing techniques, and new design strategies must be discovered in order to achieve these goals. Further research is needed to understand the underlying mechanisms, such as sample sintering processes, dielectric breakdown strength, and dielectric polarization responses in local regions, ultimately developing a profound understanding of the material–structure–property relationship of dielectric materials for energy storage. In addition to developing a single material, more attention should be paid to composite materials, for instance, ceramic/ceramic composites, ceramic/glass composites, ceramic/polymer composites, and ceramic/glass/polymer composites, because it is challenging to develop a single material with a high P_{max}, a low P_r, a high E_b, low dielectric loss, and excellent thermal stability/fatigue. Dielectric capacitors with an easy preparation technique, a simple chemical composition, and a low sintering temperature are still in great demand for practical applications. To fabricate new materials, advanced synthesis techniques (two-step sintering and pressure-assisted sintering), comprehensive characterizations (aberration-corrected scanning transmission electron microscope and piezoelectric force microscopy), various control strategies (nanodomain and grain size engineering), and theoretical calculations (machine learning and phase-field simulations) should be employed.

Ceramic-based films show an enormous performance when compared to bulk ceramics in terms of the energy storage density and dielectric breakdown strength. The energy storage properties of ceramic films have been enhanced via various methods, including solid solution formation, layered films with particular configurations (such as sandwich structures, positive/negative gradient compositions), the interface design of films/electrodes, the lattice/strain engineering of films/substrates, and more. Among them, similar to bulk ceramics, the fundamental solution is to deeply understand the inherent nature of whether AFEs/RFEs. Developing films for energy storage is challenging due to their restricted thickness and low absolute energy content. Developing various stratification and flexible scroll technologies is a viable solution for increasing the volume without losing their characteristics. Technological simplicity has the ability to accelerate manufacturing processes and boost automation, thus leading to cost savings and innovation.

MLCCs play an important role in dielectric energy storage. The macroproperties of MLCCs are mostly determined by the thickness of the dielectric layer in addition to their composition. Developing layer thinning techniques is crucial for increasing the energy density per volume. Furthermore, the expensive cost of metal electrodes, such as Au, Pt, and Ag, hinders the commercialization of MLCCs. Low-cost electrodes must be compatible with dielectrics, taking into account the sintering temperature, metal melting temperature, and interface reaction. Therefore, economical electrodes and appropriate cofire techniques should be developed. Since different metals are typically doped to internal and terminal electrodes in most cases, the method for joint connections between these electrodes should be a crucial consideration.

5. Conclusions

Dielectric materials with high power density and ultra-fast discharge rates are becoming increasingly significant in advanced electronic devices and pulsed power systems. Currently, dielectric energy-storage materials are limited in their applications due to their low energy density. Therefore, dielectric materials with excellent energy storage performance are needed. In this review paper, we discuss the fundamental concepts for energy storage in dielectric capacitors, including principles, key parameters, and influence factors for enhancing the energy storage properties. In addition, we summarize the recent progress of dielectrics, such as bulk ceramics/composites, ceramic films, and multilayer ceramic capacitors, followed by the best strategies, such as chemical modification, grain refinement, and defect engineering, for achieving a higher energy density/BDS and higher energy efficiency in dielectric materials for applications in pulsed power systems. Moreover, we present challenges and opportunities for future energy storage dielectric materials.

Author Contributions: Conceptualization, writing—original draft preparation, review, and editing, S.P.; visualization, Y.L., Y.H.S. and Y.M.B.; Review, and editing, M.P.; Validation, project administration, supervision, writing—review and editing, G.-T.H. All authors have read and agreed to the published version of the manuscript.

Funding: The work at PKNU was supported by the National Research Foundation of Korea (NRF-2022R1A2C4001497) grant funded by the Ministry of Science and ICT (MSIT) and he Pukyong National University Industry-university Cooperation Research Fund in 2023(202312480001).

Institutional Review Board Statement: Not applicable.

Informed Consent Statement: Not applicable.

Data Availability Statement: Not applicable.

Conflicts of Interest: The authors declare no conflicts of interest.

References

1. Yao, Z.; Song, Z.; Hao, H.; Yu, Z.; Cao, M.; Zhang, S.; Lanagan, M.T.; Liu, H. Homogeneous/Inhomogeneous-Structured Dielectrics and Their Energy-Storage Performances. *Adv. Mater.* **2017**, *29*, 1601727. [CrossRef]
2. Kang, B.; Ceder, G. Battery Materials for Ultrafast Charging and Discharging. *Nature* **2009**, *458*, 190–193. [CrossRef]
3. Luo, X.; Wang, J.; Dooner, M.; Clarke, J. Overview of Current Development in Electrical Energy Storage Technologies and the Application Potential in Power System Operation. *Appl. Energy* **2015**, *137*, 511–536. [CrossRef]
4. Kumar, N.; Ionin, A.; Ansell, T.; Kwon, S.; Hackenberger, W.; Cann, D. Multilayer Ceramic Capacitors Based on Relaxor $BaTiO_3$-$Bi(Zn_{1/2}Ti_{1/2})O_3$ for Temperature Stable and High Energy Density Capacitor Applications. *Appl. Phys. Lett.* **2015**, *106*, 252901. [CrossRef]
5. Li, J.; Li, F.; Xu, Z.; Zhang, S. Multilayer Lead-Free Ceramic Capacitors with Ultrahigh Energy Density and Efficiency. *Adv. Mater.* **2018**, *30*, 1802155. [CrossRef] [PubMed]
6. Palneedi, H.; Peddigari, M.; Hwang, G.-T.; Jeong, D.-Y.; Ryu, J. High-Performance Dielectric Ceramic Films for Energy Storage Capacitors: Progress and Outlook. *Adv. Funct. Mater.* **2018**, *28*, 1803665. [CrossRef]
7. Dong, J.; Hu, R.; Xu, X.; Chen, J.; Niu, Y.; Wang, F.; Hao, J.; Wu, K.; Wang, Q.; Wang, H. A Facile In Situ Surface-Functionalization Approach to Scalable Laminated High-Temperature Polymer Dielectrics with Ultrahigh Capacitive Performance. *Adv. Funct. Mater.* **2021**, *31*, 2102644. [CrossRef]
8. Yang, H.; Tian, J.; Lin, Y.; Ma, J. Realizing Ultra-High Energy Storage Density of Lead-Free $0.76Bi_{0.5}Na_{0.5}TiO_3$-$0.24SrTiO_3$-$Bi(Ni_{2/3}Nb_{1/3})O_3$ Ceramics under Low Electric Fields. *Chem. Eng. J.* **2021**, *418*, 129337. [CrossRef]
9. Li, Q.; Yao, F.-Z.; Liu, Y.; Zhang, G.; Wang, H.; Wang, Q. High-Temperature Dielectric Materials for Electrical Energy Storage. *Annu. Rev. Mater. Res.* **2018**, *48*, 219–243. [CrossRef]
10. Li, Q.; Chen, L.; Gadinski, M.R.; Zhang, S.; Zhang, G.; Li, H.U.; Iagodkine, E.; Haque, A.; Chen, L.-Q.; Jackson, T.N.; et al. Flexible High-Temperature Dielectric Materials from Polymer Nanocomposites. *Nature* **2015**, *523*, 576–579. [CrossRef]
11. Choi, H.; Ryu, J.; Yoon, W.-H.; Hwang, G.-T. Recent Progress in Dielectric-Based Ultrafast Charging/Discharging Devices. *J. Korean Inst. Electr. Electron. Mater. Eng.* **2022**, *35*, 322–332.
12. Tang, H.; Lin, Y.; Sodano, H.A. Synthesis of High Aspect Ratio $BaTiO_3$ Nanowires for High Energy Density Nanocomposite Capacitors. *Adv. Energy Mater.* **2013**, *3*, 451–456. [CrossRef]
13. Pandya, S.; Wilbur, J.; Kim, J.; Gao, R.; Dasgupta, A.; Dames, C.; Martin, L.W. Pyroelectric Energy Conversion with Large Energy and Power Density in Relaxor Ferroelectric Thin Films. *Nat. Mater.* **2018**, *17*, 432–438. [CrossRef] [PubMed]
14. Lin, Y.; Li, D.; Zhang, M.; Zhan, S.; Yang, Y.; Yang, H.; Yuan, Q. Excellent Energy-Storage Properties Achieved in $BaTiO_3$-Based Lead-Free Relaxor Ferroelectric Ceramics via Domain Engineering on the Nanoscale. *ACS Appl. Mater. Interfaces* **2019**, *11*, 36824–36830. [CrossRef] [PubMed]
15. Kishi, H.; Mizuno, Y.; Chazono, H. Base-Metal Electrode-Multilayer Ceramic Capacitors: Past, Present and Future Perspectives. *JPN J. Appl. Phys.* **2003**, *42*, 1. [CrossRef]
16. Wang, Y.; Cui, J.; Wang, L.; Yuan, Q.; Niu, Y.; Chen, J.; Wang, Q.; Wang, H. Compositional Tailoring Effect on Electric Field Distribution for Significantly Enhanced Breakdown Strength and Restrained Conductive Loss in Sandwich-Structured Ceramic/Polymer Nanocomposites. *J. Mater. Chem. A Mater.* **2017**, *5*, 4710–4718. [CrossRef]
17. Yao, F.-Z.; Yuan, Q.; Wang, Q.; Wang, H. Multiscale Structural Engineering of Dielectric Ceramics for Energy Storage Applications: From Bulk to Thin Films. *Nanoscale* **2020**, *12*, 17165–17184. [CrossRef]
18. Zhang, Y.; Yang, H.; Dang, Z.; Zhan, S.; Sun, C.; Hu, G.; Lin, Y.; Yuan, Q. Multilayer Structured Poly(Vinylidene Fluoride)-Based Composite Film with Ultrahigh Breakdown Strength and Discharged Energy Density. *ACS Appl. Mater. Interfaces* **2020**, *12*, 22137–22145. [CrossRef]
19. Wang, Y.; Wang, L.; Yuan, Q.; Chen, J.; Niu, Y.; Xu, X.; Cheng, Y.; Yao, B.; Wang, Q.; Wang, H. Ultrahigh Energy Density and Greatly Enhanced Discharged Efficiency of Sandwich-Structured Polymer Nanocomposites with Optimized Spatial Organization. *Nano Energy* **2018**, *44*, 364–370. [CrossRef]
20. Zhou, M.; Liang, R.; Zhou, Z.; Yan, S.; Dong, X. Novel Sodium Niobate-Based Lead-Free Ceramics as New Environment-Friendly Energy Storage Materials with High Energy Density, High Power Density, and Excellent Stability. *ACS Sustain. Chem. Eng.* **2018**, *6*, 12755–12765. [CrossRef]
21. Chu, B.; Zhou, X.; Ren, K.; Neese, B.; Lin, M.; Wang, Q.; Bauer, F.; Zhang, Q.M. A Dielectric Polymer with High Electric Energy Density and Fast Discharge Speed. *Science* **2006**, *313*, 334–336. [CrossRef]
22. Zhu, L.-F.; Zhao, L.; Yan, Y.; Leng, H.; Li, X.; Cheng, L.-Q.; Xiong, X.; Priya, S. Composition and Strain Engineered $AgNbO_3$—Based Multilayer Capacitors for Ultra-High Energy Storage Capacity. *J. Mater. Chem. A Mater.* **2021**, *9*, 9655–9664. [CrossRef]
23. Hu, Q.; Tian, Y.; Zhu, Q.; Bian, J.; Jin, L.; Du, H.; Alikin, D.O.; Shur, V.Y.; Feng, Y.; Xu, Z.; et al. Achieve Ultrahigh Energy Storage Performance in $BaTiO_3$–$Bi(Mg_{1/2}Ti_{1/2})O_3$ Relaxor Ferroelectric Ceramics via Nano-Scale Polarization Mismatch and Reconstruction. *Nano Energy* **2020**, *67*, 104264. [CrossRef]
24. Cao, W.; Lin, R.; Chen, P.; Li, F.; Ge, B.; Song, D.; Zhang, J.; Cheng, Z.; Wang, C. Phase and Band Structure Engineering via Linear Additive in NBT-ST for Excellent Energy Storage Performance with Superior Thermal Stability. *ACS Appl. Mater. Interfaces* **2022**, *14*, 54051–54062. [CrossRef]
25. Zhang, T.; Li, W.; Zhao, Y.; Yu, Y.; Fei, W. High Energy Storage Performance of Opposite Double-Heterojunction Ferroelectricity–Insulators. *Adv. Funct. Mater.* **2018**, *28*, 1706211. [CrossRef]

26. Zhao, L.; Liu, Q.; Gao, J.; Zhang, S.; Li, J. Lead-Free Antiferroelectric Silver Niobate Tantalate with High Energy Storage Performance. *Adv. Mater.* **2017**, *29*, 1701824. [CrossRef] [PubMed]
27. Uchino, K.; Zheng, J.H.; Chen, Y.H.; Du, X.H.; Ryu, J.; Gao, Y.; Ural, S.; Priya, S.; Hirose, S. Loss Mechanisms and High Power Piezoelectrics. *J. Mater. Sci.* **2006**, *41*, 217–228. [CrossRef]
28. Zheng, J.; Takahashi, S.; Yoshikawa, S.; Uchino, K.; de Vries, J.W.C. Heat Generation in Multilayer Piezoelectric Actuators. *J. Am. Ceram. Soc.* **1996**, *79*, 3193–3198. [CrossRef]
29. Liu, F.; Li, Q.; Cui, J.; Li, Z.; Yang, G.; Liu, Y.; Dong, L.; Xiong, C.; Wang, H.; Wang, Q. High-Energy-Density Dielectric Polymer Nanocomposites with Trilayered Architecture. *Adv. Funct. Mater.* **2017**, *27*, 1606292. [CrossRef]
30. Song, Z.; Zhang, S.; Liu, H.; Hao, H.; Cao, M.; Li, Q.; Wang, Q.; Yao, Z.; Wang, Z.; Lanagan, M.T. Improved Energy Storage Properties Accompanied by Enhanced Interface Polarization in Annealed Microwave-Sintered BST. *J. Am. Ceram. Soc.* **2015**, *98*, 3212–3222. [CrossRef]
31. Liu, B.; Wang, X.; Zhang, R.; Li, L. Grain Size Effect and Microstructure Influence on the Energy Storage Properties of Fine-grained $BaTiO_3$-based Ceramics. *J. Am. Ceram. Soc.* **2017**, *100*, 3599–3607. [CrossRef]
32. Moulson, A.J.; Herbert, J.M. *Electroceramics: Materials, Properties, Applications*; Wiley: Hoboken, NJ, USA, 2003; ISBN 9780471497479.
33. Dong, G.; Ma, S.; Du, J.; Cui, J. Dielectric Properties and Energy Storage Density in ZnO-Doped $Ba_{0.3}Sr_{0.7}TiO_3$ Ceramics. *Ceram. Int.* **2009**, *35*, 2069–2075. [CrossRef]
34. Yang, Z.; Gao, F.; Du, H.; Jin, L.; Yan, L.; Hu, Q.; Yu, Y.; Qu, S.; Wei, X.; Xu, Z.; et al. Grain Size Engineered Lead-Free Ceramics with Both Large Energy Storage Density and Ultrahigh Mechanical Properties. *Nano Energy* **2019**, *58*, 768–777. [CrossRef]
35. Wu, H.; Zhuo, F.; Qiao, H.; Kodumudi Venkataraman, L.; Zheng, M.; Wang, S.; Huang, H.; Li, B.; Mao, X.; Zhang, Q. Polymer-/Ceramic-based Dielectric Composites for Energy Storage and Conversion. *Energy Environ. Mater.* **2022**, *5*, 486–514. [CrossRef]
36. Kusko, A.; Dedad, J. Stored Energy—Short-Term and Long-Term Energy Storage Methods. *IEEE Ind. Appl. Mag.* **2007**, *13*, 66–72. [CrossRef]
37. Li, W.-T.; McKenzie, D.R.; McFall, W.D.; Zhang, Q.-C.; Wiszniewski, W. Breakdown Mechanism of Al_2O_3 Based Metal-to-Metal Antifuses. *Solid. State Electron.* **2000**, *44*, 1557–1562. [CrossRef]
38. Wang, C.; Zhang, N.; Li, Q.; Yu, Y.; Zhang, J.; Li, Y.; Wang, H. Dielectric Relaxations in Rutile TiO_2. *J. Am. Ceram. Soc.* **2015**, *98*, 148–153. [CrossRef]
39. Hanzig, J.; Zschornak, M.; Nentwich, M.; Hanzig, F.; Gemming, S.; Leisegang, T.; Meyer, D.C. Strontium Titanate: An All-in-One Rechargeable Energy Storage Material. *J. Power Sources* **2014**, *267*, 700–705. [CrossRef]
40. Sarantopoulos, A.; Ferreiro-Vila, E.; Pardo, V.; Magén, C.; Aguirre, M.H.; Rivadulla, F. Electronic Degeneracy and Intrinsic Magnetic Properties of Epitaxial Nb:$SrTiO_3$ Thin Films Controlled by Defects. *Phys. Rev. Lett.* **2015**, *115*, 166801. [CrossRef]
41. Zhang, G.-F.; Liu, H.; Yao, Z.; Cao, M.; Hao, H. Effects of Ca Doping on the Energy Storage Properties of (Sr, Ca)TiO_3 Paraelectric Ceramics. *J. Mater. Sci. Mater. Electron.* **2015**, *26*, 2726–2732. [CrossRef]
42. Liu, S.; Zhai, J. Improving the Dielectric Constant and Energy Density of Poly(Vinylidene Fluoride) Composites Induced by Surface-Modified $SrTiO_3$ Nanofibers by Polyvinylpyrrolidone. *J. Mater. Chem. A Mater.* **2015**, *3*, 1511–1517. [CrossRef]
43. Shay, D.P.; Podraza, N.J.; Donnelly, N.J.; Randall, C.A. High Energy Density, High Temperature Capacitors Utilizing Mn-Doped $0.8CaTiO_3$–$0.2CaHfO_3$ Ceramics. *J. Am. Ceram. Soc.* **2012**, *95*, 1348–1355. [CrossRef]
44. Wang, Z.; Cao, M.; Yao, Z.; Li, G.; Song, Z.; Hu, W.; Hao, H.; Liu, H.; Yu, Z. Effects of Sr/Ti Ratio on the Microstructure and Energy Storage Properties of Nonstoichiometric $SrTiO_3$ Ceramics. *Ceram. Int.* **2014**, *40*, 929–933. [CrossRef]
45. Yao, Z.; Luo, Q.; Zhang, G.; Hao, H.; Cao, M.; Liu, H. Improved Energy-Storage Performance and Breakdown Enhancement Mechanism of Mg-Doped $SrTiO_3$ Bulk Ceramics for High Energy Density Capacitor Applications. *J. Mater. Sci. Mater. Electron.* **2017**, *28*, 11491–11499. [CrossRef]
46. Vorotilov, K.A.; Yanovskaya, M.I.; Solovjeva, L.I.; Valeev, A.S.; Petrovsky, V.I.; Vasiljev, V.A.; Obvinzeva, I.E. Ferroelectric Capacitors for Integrated Circuits. *Microelectron. Eng.* **1995**, *29*, 41–44. [CrossRef]
47. Cheng, B.L.; Wang, C.; Wang, S.Y.; Lu, H.B.; Zhou, Y.L.; Chen, Z.H.; Yang, G.Z. Dielectric Properties of $(Ba_{0.8}Sr_{0.2})(Zr_xTi_{1-x})O_3$ Thin Films Grown by Pulsed-Laser Deposition. *J. Eur. Ceram. Soc.* **2005**, *25*, 2295–2298. [CrossRef]
48. Ogihara, H.; Randall, C.A.; Trolier-McKinstry, S. High Temperature and High Energy Density Dielectric Materials. *J. Am. Ceram. Soc.* **2009**, *92*, 106–113.
49. Wang, Y.; Shen, Z.-Y.; Li, Y.-M.; Wang, Z.-M.; Luo, W.-Q.; Hong, Y. Optimization of Energy Storage Density and Efficiency in $Ba_xSr_{1-x}TiO_3$ ($x \leq 0.4$) Paraelectric Ceramics. *Ceram. Int.* **2015**, *41*, 8252–8256. [CrossRef]
50. Choi, H.; Pattipaka, S.; Son, Y.H.; Bae, Y.M.; Park, J.H.; Jeong, C.K.; Lee, H.E.; Kim, S.-D.; Ryu, J.; Hwang, G.-T. Improved Energy Storage Density and Efficiency of Nd and Mn Co-Doped $Ba_{0.7}Sr_{0.3}TiO_3$ Ceramic Capacitors via Defect Dipole Engineering. *Materials* **2023**, *16*, 6753. [CrossRef]
51. Luo, B.; Wang, X.; Tian, E.; Song, H.; Qu, H.; Cai, Z.; Li, B.; Li, L. Mechanism of Ferroelectric Properties of (BaCa)(ZrTi)O_3 from First-Principles Calculations. *Ceram. Int.* **2018**, *44*, 9684–9688. [CrossRef]
52. Song, Z.; Liu, H.; Zhang, S.; Wang, Z.; Shi, Y.; Hao, H.; Cao, M.; Yao, Z.; Yu, Z. Effect of Grain Size on the Energy Storage Properties of $(Ba_{0.4}Sr_{0.6})TiO_3$ Paraelectric Ceramics. *J. Eur. Ceram. Soc.* **2014**, *34*, 1209–1217. [CrossRef]

53. Tagantsev, A.K.; Vaideeswaran, K.; Vakhrushev, S.B.; Filimonov, A.V.; Burkovsky, R.G.; Shaganov, A.; Andronikova, D.; Rudskoy, A.I.; Baron, A.Q.R.; Uchiyama, H.; et al. The Origin of Antiferroelectricity in $PbZrO_3$. *Nat. Commun.* **2013**, *4*, 2229. [CrossRef] [PubMed]
54. Hao, X.; Zhai, J.; Kong, L.B.; Xu, Z. A Comprehensive Review on the Progress of Lead Zirconate-Based Antiferroelectric Materials. *Prog. Mater. Sci.* **2014**, *63*, 1–57. [CrossRef]
55. Qiao, P.; Zhang, Y.; Chen, X.; Zhou, M.; Yan, S.; Dong, X.; Wang, G. Enhanced Energy Storage Properties and Stability in $(Pb_{0.895}La_{0.07})(Zr_xTi_{1-x})O_3$ Antiferroelectric Ceramics. *Ceram. Int.* **2019**, *45*, 15898–15905. [CrossRef]
56. Dan, Y.; Zou, K.; Chen, G.; Yu, Y.; Zhang, Y.; Zhang, Q.; Lu, Y.; Zhang, Q.; He, Y. Superior Energy-Storage Properties in $(Pb,La)(Zr,Sn,Ti)O_3$ Antiferroelectric Ceramics with Appropriate La Content. *Ceram. Int.* **2019**, *45*, 11375–11381. [CrossRef]
57. Pan, W.; Zhang, Q.; Bhalla, A.; Cross, L.E. Field-Forced Antiferroelectric-to-Ferroelectric Switching in Modified Lead Zirconate Titanate Stannate Ceramics. *J. Am. Ceram. Soc.* **1989**, *72*, 571–578. [CrossRef]
58. Wang, H.; Liu, Y.; Yang, T.; Zhang, S. Ultrahigh Energy-Storage Density in Antiferroelectric Ceramics with Field-Induced Multiphase Transitions. *Adv. Funct. Mater.* **2019**, *29*, 1807321. [CrossRef]
59. Liu, X.; Li, Y.; Hao, X. Ultra-High Energy-Storage Density and Fast Discharge Speed of $(Pb_{0.98-x}La_{0.02}Sr_x)(Zr_{0.9}Sn_{0.1})_{0.995}O_3$ Antiferroelectric Ceramics Prepared via the Tape-Casting Method. *J. Mater. Chem. A Mater.* **2019**, *7*, 11858–11866. [CrossRef]
60. Luo, N.; Han, K.; Zhuo, F.; Xu, C.; Zhang, G.; Liu, L.; Chen, X.; Hu, C.; Zhou, H.; Wei, Y. Aliovalent A-Site Engineered $AgNbO_3$ Lead-Free Antiferroelectric Ceramics toward Superior Energy Storage Density. *J. Mater. Chem. A Mater.* **2019**, *7*, 14118–14128. [CrossRef]
61. Han, K.; Luo, N.; Mao, S.; Zhuo, F.; Liu, L.; Peng, B.; Chen, X.; Hu, C.; Zhou, H.; Wei, Y. Ultrahigh Energy-Storage Density in A-/B-Site Co-Doped $AgNbO_3$ Lead-Free Antiferroelectric Ceramics: Insight into the Origin of Antiferroelectricity. *J. Mater. Chem. A Mater.* **2019**, *7*, 26293–26301. [CrossRef]
62. Luo, N.; Han, K.; Zhuo, F.; Liu, L.; Chen, X.; Peng, B.; Wang, X.; Feng, Q.; Wei, Y. Design for High Energy Storage Density and Temperature-Insensitive Lead-Free Antiferroelectric Ceramics. *J. Mater. Chem. C Mater.* **2019**, *7*, 4999–5008. [CrossRef]
63. Luo, N.; Han, K.; Cabral, M.J.; Liao, X.; Zhang, S.; Liao, C.; Zhang, G.; Chen, X.; Feng, Q.; Li, J.-F.; et al. Constructing Phase Boundary in $AgNbO_3$ Antiferroelectrics: Pathway Simultaneously Achieving High Energy Density and Efficiency. *Nat. Commun.* **2020**, *11*, 4824. [CrossRef] [PubMed]
64. Qi, H.; Zuo, R. Linear-like Lead-Free Relaxor Antiferroelectric $(Bi_{0.5}Na_{0.5})TiO_3$–$NaNbO_3$ with Giant Energy-Storage Density/Efficiency and Super Stability against Temperature and Frequency. *J. Mater. Chem. A Mater.* **2019**, *7*, 3971–3978. [CrossRef]
65. Qi, H.; Zuo, R.; Xie, A.; Tian, A.; Fu, J.; Zhang, Y.; Zhang, S. Ultrahigh Energy-Storage Density in $NaNbO_3$-Based Lead-Free Relaxor Antiferroelectric Ceramics with Nanoscale Domains. *Adv. Funct. Mater.* **2019**, *29*, 1903877. [CrossRef]
66. Wang, J.; Wan, X.; Rao, Y.; Zhao, L.; Zhu, K. Hydrothermal Synthesized $AgNbO_3$ Powders: Leading to Greatly Improved Electric Breakdown Strength in Ceramics. *J. Eur. Ceram. Soc.* **2020**, *40*, 5589–5596. [CrossRef]
67. Smolenskii, G.A.; Isupov, V.A.; Agranovskaya, A.I.; Popov, S.N. Ferroelectrics with Diffuse Phase Transitions. *Sov. Phys.-Solid. State* **1961**, *2*, 2584–2594. [CrossRef]
68. Shvartsman, V.V.; Lupascu, D.C. Lead-Free Relaxor Ferroelectrics. *J. Am. Ceram. Soc.* **2012**, *95*, 1–26. [CrossRef]
69. Perumal, R.N.; Athikesavan, V. Investigations on Electrical and Energy Storage Behaviour of PZN-PT, PMN-PT, PZN–PMN-PT Piezoelectric Solid Solutions. *J. Mater. Sci. Mater. Electron.* **2019**, *30*, 902–913. [CrossRef]
70. Zhang, T.F.; Tang, X.G.; Liu, Q.X.; Jiang, Y.P.; Huang, X.X.; Zhou, Q.F. Energy-Storage Properties and High-Temperature Dielectric Relaxation Behaviors of Relaxor Ferroelectric $Pb(Mg_{1/3}Nb_{2/3})O_3$–$PbTiO_3$ Ceramics. *J. Phys. D Appl. Phys.* **2016**, *49*, 095302. [CrossRef]
71. Cross, L.E. Relaxorferroelectrics: An Overview. *Ferroelectrics* **1994**, *151*, 305–320. [CrossRef]
72. Liu, G.; Li, Y.; Guo, B.; Tang, M.; Li, Q.; Dong, J.; Yu, L.; Yu, K.; Yan, Y.; Wang, D.; et al. Ultrahigh Dielectric Breakdown Strength and Excellent Energy Storage Performance in Lead-Free Barium Titanate-Based Relaxor Ferroelectric Ceramics via a Combined Strategy of Composition Modification, Viscous Polymer Processing, and Liquid-Phase Sintering. *Chem. Eng. J.* **2020**, *398*, 125625. [CrossRef]
73. Triamnak, N.; Yimnirun, R.; Pokorny, J.; Cann, D.P. Relaxor Characteristics of the Phase Transformation in $(1-x)BaTiO_3$–$xBi(Zn_{1/2}Ti_{1/2})O_3$ Perovskite Ceramics. *J. Am. Ceram. Soc.* **2013**, *96*, 3176–3182. [CrossRef]
74. Yang, H.; Lu, Z.; Li, L.; Bao, W.; Ji, H.; Li, J.; Feteira, A.; Xu, F.; Zhang, Y.; Sun, H.; et al. Novel $BaTiO_3$-Based, Ag/Pd-Compatible Lead-Free Relaxors with Superior Energy Storage Performance. *ACS Appl. Mater. Interfaces* **2020**, *12*, 43942–43949. [CrossRef] [PubMed]
75. Ibn-Mohammed, T.; Koh, S.C.L.; Reaney, I.M.; Sinclair, D.C.; Mustapha, K.B.; Acquaye, A.; Wang, D. Are Lead-Free Piezoelectrics More Environmentally Friendly? *MRS Commun.* **2017**, *7*, 1–7. [CrossRef]
76. Ibn-Mohammed, T.; Koh, S.C.L.; Reaney, I.M.; Acquaye, A.; Wang, D.; Taylor, S.; Genovese, A. Integrated Hybrid Life Cycle Assessment and Supply Chain Environmental Profile Evaluations of Lead-Based (Lead Zirconate Titanate) versus Lead-Free (Potassium Sodium Niobate) Piezoelectric Ceramics. *Energy Environ. Sci.* **2016**, *9*, 3495–3520. [CrossRef]
77. Khodorov, A.; Pereira, M.; Gomes, M.J.M. Structure and Dielectric Properties of Sol–Gel 9/65/35 PLZT Thin Films. *J. Eur. Ceram. Soc.* **2005**, *25*, 2285–2288. [CrossRef]
78. Hao, X.; Wang, Y.; Yang, J.; An, S.; Xu, J. High Energy-Storage Performance in $Pb_{0.91}La_{0.09}(Ti_{0.65}Zr_{0.35})O_3$ Relaxor Ferroelectric Thin Films. *J. Appl. Phys.* **2012**, *112*, 114111. [CrossRef]

79. Zhang, L.; Hao, X.; Yang, J.; An, S.; Song, B. Large Enhancement of Energy-Storage Properties of Compositional Graded $(Pb_{1-x}La_x)(Zr_{0.65}Ti_{0.35})O_3$ Relaxor Ferroelectric Thick Films. *Appl. Phys. Lett.* **2013**, *103*, 113902. [CrossRef]
80. Liu, Y.; Hao, X.; An, S. Significant Enhancement of Energy-Storage Performance of $(Pb_{0.91}La_{0.09})(Zr_{0.65}Ti_{0.35})O_3$ Relaxor Ferroelectric Thin Films by Mn Doping. *J. Appl. Phys.* **2013**, *114*, 174102. [CrossRef]
81. Zhao, Q.L.; Cao, M.S.; Yuan, J.; Lu, R.; Wang, D.W.; Zhang, D.Q. Thickness Effect on Electrical Properties of $Pb(Zr_{0.52}Ti_{0.48})O_3$ Thick Films Embedded with ZnO Nanowhiskers Prepared by a Hybrid Sol–Gel Route. *Mater. Lett.* **2010**, *64*, 632–635. [CrossRef]
82. Yang, L.; Kong, X.; Li, F.; Hao, H.; Cheng, Z.; Liu, H.; Li, J.-F.; Zhang, S. Perovskite Lead-Free Dielectrics for Energy Storage Applications. *Prog. Mater. Sci.* **2019**, *102*, 72–108. [CrossRef]
83. Xie, Z.; Peng, B.; Zhang, J.; Zhang, X.; Yue, Z.; Li, L. Highly (100)-Oriented $Bi(Ni_{1/2}Hf_{1/2})O_3$-$PbTiO_3$ Relaxor-Ferroelectric Films for Integrated Piezoelectric Energy Harvesting and Storage System. *J. Am. Ceram. Soc.* **2015**, *98*, 2968–2971. [CrossRef]
84. Xie, Z.; Yue, Z.; Peng, B.; Zhang, J.; Zhao, C.; Zhang, X.; Ruehl, G.; Li, L. Large Enhancement of the Recoverable Energy Storage Density and Piezoelectric Response in Relaxor-Ferroelectric Capacitors by Utilizing the Seeding Layers Engineering. *Appl. Phys. Lett.* **2015**, *106*, 202901. [CrossRef]
85. Wang, X.; Zhang, L.; Hao, X.; An, S. High Energy-Storage Performance of $0.9Pb(Mg_{1/3}Nb_{2/3})O_3$-$0.1PbTiO_3$ Relaxor Ferroelectric Thin Films Prepared by RF Magnetron Sputtering. *Mater. Res. Bull.* **2015**, *65*, 73–79. [CrossRef]
86. Ogihara, H.; Randall, C.A.; Trolier-McKinstry, S. High-Energy Density Capacitors Utilizing $0.7BaTiO_3$–0.3 $BiScO_3$ Ceramics. *J. Am. Ceram. Soc.* **2009**, *92*, 1719–1724. [CrossRef]
87. Shen, Z.; Wang, X.; Luo, B.; Li, L. $BaTiO_3$–$BiYbO_3$ Perovskite Materials for Energy Storage Applications. *J. Mater. Chem. A Mater.* **2015**, *3*, 18146–18153. [CrossRef]
88. Li, W.-B.; Zhou, D.; Pang, L.-X.; Xu, R.; Guo, H.-H. Novel Barium Titanate Based Capacitors with High Energy Density and Fast Discharge Performance. *J. Mater. Chem. A Mater.* **2017**, *5*, 19607–19612. [CrossRef]
89. Zhang, L.; Pang, L.-X.; Li, W.-B.; Zhou, D. Extreme High Energy Storage Efficiency in Perovskite Structured $(1-x)(Ba_{0.8}Sr_{0.2})TiO_3$-$xBi(Zn_{2/3}Nb_{1/3})O_3$ $(0.04 \leq x \leq 0.16)$ Ceramics. *J. Eur. Ceram. Soc.* **2020**, *40*, 3343–3347. [CrossRef]
90. Yuan, Q.; Yao, F.; Wang, Y.; Ma, R.; Wang, H. Relaxor Ferroelectric $0.9BaTiO_3$–$0.1Bi(Zn_{0.5}Zr_{0.5})O_3$ Ceramic Capacitors with High Energy Density and Temperature Stable Energy Storage Properties. *J. Mater. Chem. C Mater.* **2017**, *5*, 9552–9558. [CrossRef]
91. Zhou, M.; Liang, R.; Zhou, Z.; Dong, X. Novel $BaTiO_3$-Based Lead-Free Ceramic Capacitors Featuring High Energy Storage Density, High Power Density, and Excellent Stability. *J. Mater. Chem. C Mater.* **2018**, *6*, 8528–8537. [CrossRef]
92. Li, F.; Zhou, M.; Zhai, J.; Shen, B.; Zeng, H. Novel Barium Titanate Based Ferroelectric Relaxor Ceramics with Superior Charge-Discharge Performance. *J. Eur. Ceram. Soc.* **2018**, *38*, 4646–4652. [CrossRef]
93. Yuan, Q.; Li, G.; Yao, F.-Z.; Cheng, S.-D.; Wang, Y.; Ma, R.; Mi, S.-B.; Gu, M.; Wang, K.; Li, J.-F.; et al. Simultaneously Achieved Temperature-Insensitive High Energy Density and Efficiency in Domain Engineered $BaTiO_3$-$Bi(Mg_{0.5}Zr_{0.5})O_3$ Lead-Free Relaxor Ferroelectrics. *Nano Energy* **2018**, *52*, 203–210. [CrossRef]
94. Liu, N.; Liang, R.; Zhou, Z.; Dong, X. Designing Lead-Free Bismuth Ferrite-Based Ceramics Learning from Relaxor Ferroelectric Behavior for Simultaneous High Energy Density and Efficiency under Low Electric Field. *J. Mater. Chem. C Mater.* **2018**, *6*, 10211–10217. [CrossRef]
95. Qiao, X.; Zhang, F.; Wu, D.; Chen, B.; Zhao, X.; Peng, Z.; Ren, X.; Liang, P.; Chao, X.; Yang, Z. Superior Comprehensive Energy Storage Properties in $Bi_{0.5}Na_{0.5}TiO_3$-Based Relaxor Ferroelectric Ceramics. *Chem. Eng. J.* **2020**, *388*, 124158. [CrossRef]
96. Yan, F.; Huang, K.; Jiang, T.; Zhou, X.; Shi, Y.; Ge, G.; Shen, B.; Zhai, J. Significantly Enhanced Energy Storage Density and Efficiency of BNT-Based Perovskite Ceramics via A-Site Defect Engineering. *Energy Storage Mater.* **2020**, *30*, 392–400. [CrossRef]
97. Zhang, X.; Hu, D.; Pan, Z.; Lv, X.; He, Z.; Yang, F.; Li, P.; Liu, J.; Zhai, J. Enhancement of Recoverable Energy Density and Efficiency of Lead-Free Relaxor-Ferroelectric BNT-Based Ceramics. *Chem. Eng. J.* **2021**, *406*, 126818. [CrossRef]
98. Wu, Y.; Fan, Y.; Liu, N.; Peng, P.; Zhou, M.; Yan, S.; Cao, F.; Dong, X.; Wang, G. Enhanced Energy Storage Properties in Sodium Bismuth Titanate-Based Ceramics for Dielectric Capacitor Applications. *J. Mater. Chem. C Mater.* **2019**, *7*, 6222–6230. [CrossRef]
99. Liu, X.; Rao, R.; Shi, J.; He, J.; Zhao, Y.; Liu, J.; Du, H. Effect of Oxygen Vacancy and A-Site-Deficiency on the Dielectric Performance of BNT-BT-BST Relaxors. *J. Alloys Compd.* **2021**, *875*, 159999. [CrossRef]
100. Pattipaka, S.; Choi, H.; Lim, Y.; Park, K.-I.; Chung, K.; Hwang, G.-T. Enhanced Energy Storage Performance and Efficiency in $Bi_{0.5}(Na_{0.8}K_{0.2})_{0.5}TiO_3$-$Bi_{0.2}Sr_{0.7}TiO_3$ Relaxor Ferroelectric Ceramics via Domain Engineering. *Materials* **2023**, *16*, 4912. [CrossRef]
101. Ma, W.; Zhu, Y.; Marwat, M.A.; Fan, P.; Xie, B.; Salamon, D.; Ye, Z.-G.; Zhang, H. Enhanced Energy-Storage Performance with Excellent Stability under Low Electric Fields in BNT–ST Relaxor Ferroelectric Ceramics. *J. Mater. Chem. C Mater.* **2019**, *7*, 281–288. [CrossRef]
102. Yang, Z.; Du, H.; Qu, S.; Hou, Y.; Ma, H.; Wang, J.; Wang, J.; Wei, X.; Xu, Z. Significantly Enhanced Recoverable Energy Storage Density in Potassium–Sodium Niobate-Based Lead Free Ceramics. *J. Mater. Chem. A Mater.* **2016**, *4*, 13778–13785. [CrossRef]
103. Shao, T.; Du, H.; Ma, H.; Qu, S.; Wang, J.; Wang, J.; Wei, X.; Xu, Z. Potassium–Sodium Niobate Based Lead-Free Ceramics: Novel Electrical Energy Storage Materials. *J. Mater. Chem. A Mater.* **2017**, *5*, 554–563. [CrossRef]
104. Qu, B.; Du, H.; Yang, Z.; Liu, Q.; Liu, T. Enhanced Dielectric Breakdown Strength and Energy Storage Density in Lead-Free Relaxor Ferroelectric Ceramics Prepared Using Transition Liquid Phase Sintering. *RSC Adv.* **2016**, *6*, 34381–34389. [CrossRef]
105. Xie, A.; Zuo, R.; Qiao, Z.; Fu, Z.; Hu, T.; Fei, L. $NaNbO_3$-$(Bi_{0.5}Li_{0.5})TiO_3$ Lead-Free Relaxor Ferroelectric Capacitors with Superior Energy-Storage Performances via Multiple Synergistic Design. *Adv. Energy Mater.* **2021**, *11*, 2101378. [CrossRef]

106. Wang, W.; Pu, Y.; Guo, X.; Shi, R.; Yang, M.; Li, J. Enhanced Energy Storage and Fast Charge-Discharge Capability in $Ca_{0.5}Sr_{0.5}TiO_3$-Based Linear Dielectric Ceramic. *J. Alloys Compd.* **2020**, *817*, 152695. [CrossRef]
107. Wang, W.; Pu, Y.; Guo, X.; Shi, R.; Yang, M.; Li, J. Combining High Energy Efficiency and Fast Charge-Discharge Capability in Calcium Strontium Titanate-Based Linear Dielectric Ceramic for Energy-Storage. *Ceram. Int.* **2020**, *46*, 11484–11491. [CrossRef]
108. Wang, W.; Pu, Y.; Guo, X.; Shi, R.; Shi, Y.; Yang, M.; Li, J.; Peng, X.; Li, Y. Enhanced Energy Storage Density and High Efficiency of Lead-Free $Ca_{1-x}Sr_xTi_{1-y}Zr_yO_3$ Linear Dielectric Ceramics. *J. Eur. Ceram. Soc.* **2019**, *39*, 5236–5242. [CrossRef]
109. Wang, W.; Pu, Y.; Guo, X.; Ouyang, T.; Shi, Y.; Yang, M.; Li, J.; Shi, R.; Liu, G. Enhanced Energy Storage Properties of Lead-Free $(Ca_{0.5}Sr_{0.5})_{1-1.5x}La_xTiO_3$ Linear Dielectric Ceramics within a Wide Temperature Range. *Ceram. Int.* **2019**, *45*, 14684–14690. [CrossRef]
110. Li, F.; Si, R.; Li, T.; Wang, C.; Zhai, J. High Energy Storage Performance and Fast Discharging Speed in Dense $0.7Bi_{0.5}K_{0.5}TiO_3$-$0.3SrTiO_3$ Ceramics via a Novel Rolling Technology. *Ceram. Int.* **2020**, *46*, 6995–6998. [CrossRef]
111. Ouyang, T.; Pu, Y.; Ji, J.; Zhou, S.; Li, R. Ultrahigh Energy Storage Capacity with Superfast Discharge Rate Achieved in Mg-Modified $Ca_{0.5}Sr_{0.5}TiO_3$-Based Lead-Free Linear Ceramics for Dielectric Capacitor Applications. *Ceram. Int.* **2021**, *47*, 20447–20455. [CrossRef]
112. Pu, Y.; Wang, W.; Guo, X.; Shi, R.; Yang, M.; Li, J. Enhancing the Energy Storage Properties of $Ca_{0.5}Sr_{0.5}TiO_3$-Based Lead-Free Linear Dielectric Ceramics with Excellent Stability through Regulating Grain Boundary Defects. *J. Mater. Chem. C Mater.* **2019**, *7*, 14384–14393. [CrossRef]
113. Ding, Y.; Li, P.; He, J.; Que, W.; Bai, W.; Zheng, P.; Zhang, J.; Zhai, J. Simultaneously Achieving High Energy-Storage Efficiency and Density in Bi-Modified $SrTiO_3$-Based Relaxor Ferroelectrics by Ion Selective Engineering. *Compos. B Eng.* **2022**, *230*, 109493. [CrossRef]
114. Yu, Z.; Zeng, J.; Zheng, L.; Rousseau, A.; Li, G.; Kassiba, A. Microstructure Effects on the Energy Storage Density in $BiFeO_3$-Based Ferroelectric Ceramics. *Ceram. Int.* **2021**, *47*, 12735–12741. [CrossRef]
115. Balmuchu, S.P.; Malapati, V.; Chilaka, R.R.; Dobbidi, P. Effective Strategy for Achieving Superior Energy Storage Performance in Lead-Free $BaTiO_3$–$Bi(Zn_{2/3}(Nb_{0.85}Ta_{0.15})_{1/3})O_3$ Ferroelectric Ceramics. *Ceram. Int.* **2024**, *50*, 13782–13793. [CrossRef]
116. Liu, Z.-G.; Li, M.-D.; Tang, Z.-H.; Tang, X.-G. Enhanced Energy Storage Density and Efficiency in Lead-Free $Bi(Mg_{1/2}Hf_{1/2})O_3$-Modified $BaTiO_3$ Ceramics. *Chem. Eng. J.* **2021**, *418*, 129379. [CrossRef]
117. Huang, K.; Ge, G.; Yan, F.; Shen, B.; Zhai, J. Ultralow Electrical Hysteresis along with High Energy-Storage Density in Lead-Based Antiferroelectric Ceramics. *Adv. Electron. Mater.* **2020**, *6*, 1901366. [CrossRef]
118. Huang, J.; Qi, H.; Gao, Y.; Xie, A.; Zhang, Y.; Li, Y.; Wang, S.; Zuo, R. Expanded Linear Polarization Response and Excellent Energy-Storage Properties in $(Bi_{0.5}Na_{0.5})TiO_3$-$KNbO_3$ Relaxor Antiferroelectrics with Medium Permittivity. *Chem. Eng. J.* **2020**, *398*, 125639. [CrossRef]
119. Li, S.; Hu, T.; Nie, H.; Fu, Z.; Xu, C.; Xu, F.; Wang, G.; Dong, X. Giant Energy Density and High Efficiency Achieved in Silver Niobate-Based Lead-Free Antiferroelectric Ceramic Capacitors via Domain Engineering. *Energy Storage Mater.* **2021**, *34*, 417–426. [CrossRef]
120. Lu, Z.; Bao, W.; Wang, G.; Sun, S.-K.; Li, L.; Li, J.; Yang, H.; Ji, H.; Feteira, A.; Li, D.; et al. Mechanism of Enhanced Energy Storage Density in $AgNbO_3$-Based Lead-Free Antiferroelectrics. *Nano Energy* **2021**, *79*, 105423. [CrossRef]
121. Lai, D.; Yao, Z.; You, W.; Gao, B.; Guo, Q.; Lu, P.; Ullah, A.; Hao, H.; Cao, M.; Liu, H. Modulating the Energy Storage Performance of $NaNbO_3$-Based Lead-Free Ceramics for Pulsed Power Capacitors. *Ceram. Int.* **2020**, *46*, 13511–13516. [CrossRef]
122. Dong, X.; Li, X.; Chen, X.; Chen, H.; Sun, C.; Shi, J.; Pang, F.; Zhou, H. High Energy Storage and Ultrafast Discharge in $NaNbO_3$-Based Lead-Free Dielectric Capacitors via a Relaxor Strategy. *Ceram. Int.* **2021**, *47*, 3079–3088. [CrossRef]
123. Chen, J.; Qi, H.; Zuo, R. Realizing Stable Relaxor Antiferroelectric and Superior Energy Storage Properties in $(Na_{1-x/2}La_{x/2})(Nb_{1-x}Ti_x)O_3$ Lead-Free Ceramics through A/B-Site Complex Substitution. *ACS Appl. Mater. Interfaces* **2020**, *12*, 32871–32879. [CrossRef] [PubMed]
124. Chen, H.; Shi, J.; Chen, X.; Sun, C.; Pang, F.; Dong, X.; Zhang, H.; Zhou, H. Excellent Energy Storage Properties and Stability of $NaNbO_3$–$Bi(Mg_{0.5}Ta_{0.5})O_3$ Ceramics by Introducing $(Bi_{0.5}Na_{0.5})_{0.7}Sr_{0.3}TiO_3$. *J. Mater. Chem. A Mater.* **2021**, *9*, 4789–4799. [CrossRef]
125. Dong, X.; Chen, H.; Wei, M.; Wu, K.; Zhang, J. Structure, Dielectric and Energy Storage Properties of $BaTiO_3$ Ceramics Doped with $YNbO_4$. *J. Alloys Compd.* **2018**, *744*, 721–727. [CrossRef]
126. Akram, F.; Kim, J.; Khan, S.A.; Zeb, A.; Yeo, H.G.; Sung, Y.S.; Song, T.K.; Kim, M.-H.; Lee, S. Less Temperature-Dependent High Dielectric and Energy-Storage Properties of Eco-Friendly $BiFeO_3$–$BaTiO_3$-Based Ceramics. *J. Alloys Compd.* **2020**, *818*, 152878. [CrossRef]
127. Meng, D.; Feng, Q.; Luo, N.; Yuan, C.; Zhou, C.; Wei, Y.; Fujita, T.; You, H.; Chen, G. Effect of $Sr(Zn_{1/3}Nb_{2/3})O_3$ Modification on the Energy Storage Performance of BaTiO3 Ceramics. *Ceram. Int.* **2021**, *47*, 12450–12458. [CrossRef]
128. Zhou, M.; Liang, R.; Zhou, Z.; Dong, X. Combining High Energy Efficiency and Fast Charge-Discharge Capability in Novel $BaTiO_3$-Based Relaxor Ferroelectric Ceramic for Energy-Storage. *Ceram. Int.* **2019**, *45*, 3582–3590. [CrossRef]
129. Zeng, X.; Li, Y.; Dong, J.; Li, J.; Yang, Z.; Song, C.; Liu, G.; Yan, Y. The Polarization Contribution and Effect Mechanism of Ce-Doped $0.65BaTiO_3$-$0.35Sr_{0.7}Bi_{0.2}TiO_3$ Pb-Free Ferroelectric Ceramics for Dielectric Energy Storage. *Ceram. Int.* **2021**, *47*, 32015–32024. [CrossRef]
130. Li, Y.; Liu, Y.; Tang, M.; Lv, J.; Chen, F.; Li, Q.; Yan, Y.; Wu, F.; Jin, L.; Liu, G. Energy Storage Performance of $BaTiO_3$-Based Relaxor Ferroelectric Ceramics Prepared through a Two-Step Process. *Chem. Eng. J.* **2021**, *419*, 129673. [CrossRef]

131. Zhu, C.; Cai, Z.; Luo, B.; Guo, L.; Li, L.; Wang, X. High Temperature Lead-Free BNT-Based Ceramics with Stable Energy Storage and Dielectric Properties. *J. Mater. Chem. A Mater.* **2020**, *8*, 683–692. [CrossRef]
132. Yang, L.; Kong, X.; Cheng, Z.; Zhang, S. Ultra-High Energy Storage Performance with Mitigated Polarization Saturation in Lead-Free Relaxors. *J. Mater. Chem. A Mater.* **2019**, *7*, 8573–8580. [CrossRef]
133. Luo, C.; Feng, Q.; Luo, N.; Yuan, C.; Zhou, C.; Wei, Y.; Fujita, T.; Xu, J.; Chen, G. Effect of Ca^{2+}/Hf^{4+} Modification at A/B Sites on Energy-Storage Density of $Bi_{0.47}Na_{0.47}Ba_{0.06}TiO_3$ Ceramics. *Chem. Eng. J.* **2021**, *420*, 129861. [CrossRef]
134. Yang, F.; Bao, S.; Zhai, Y.; Zhang, Y.; Su, Z.; Liu, J.; Zhai, J.; Pan, Z. Enhanced Energy-Storage Performance and Thermal Stability in $Bi_{0.5}Na_{0.5}TiO_3$-Based Ceramics through Defect Engineering and Composition Design. *Mater. Today Chem.* **2021**, *22*, 100583. [CrossRef]
135. Li, D.; Zhou, D.; Liu, W.; Wang, P.-J.; Guo, Y.; Yao, X.-G.; Lin, H.-X. Enhanced Energy Storage Properties Achieved in $Na_{0.5}Bi_{0.5}TiO_3$-Based Ceramics via Composition Design and Domain Engineering. *Chem. Eng. J.* **2021**, *419*, 129601. [CrossRef]
136. Yan, F.; Zhou, X.; He, X.; Bai, H.; Wu, S.; Shen, B.; Zhai, J. Superior Energy Storage Properties and Excellent Stability Achieved in Environment-Friendly Ferroelectrics via Composition Design Strategy. *Nano Energy* **2020**, *75*, 105012. [CrossRef]
137. Yan, F.; Bai, H.; Zhou, X.; Ge, G.; Li, G.; Shen, B.; Zhai, J. Realizing Superior Energy Storage Properties in Lead-Free Ceramics via a Macro-Structure Design Strategy. *J. Mater. Chem. A Mater.* **2020**, *8*, 11656–11664. [CrossRef]
138. Manan, A.; Ullah, A.; Khan, M.A.; Ahmad, A.S.; Iqbal, Y.; Qazi, I.; Rehman, M.U.; Ullah, A.; Liu, H. Preparation, Characterization, and Improvement in the Energy Storage Properties of $Bi(Li_{0.5}Ta_{0.5})O_3$ Modified $Na_{0.5}K_{0.5}NbO_3$ Ceramic System. *Mater. Res. Bull.* **2022**, *145*, 111521. [CrossRef]
139. Ren, X.; Jin, L.; Peng, Z.; Chen, B.; Qiao, X.; Wu, D.; Li, G.; Du, H.; Yang, Z.; Chao, X. Regulation of Energy Density and Efficiency in Transparent Ceramics by Grain Refinement. *Chem. Eng. J.* **2020**, *390*, 124566. [CrossRef]
140. Huan, Y.; Wei, T.; Wang, X.; Liu, X.; Zhao, P.; Wang, X. Achieving Ultrahigh Energy Storage Efficiency in Local-Composition Gradient-Structured Ferroelectric Ceramics. *Chem. Eng. J.* **2021**, *425*, 129506. [CrossRef]
141. Zhang, Y.; Zuo, R. Excellent Energy-Storage Performances in La_2O_3 Doped (Na,K)NbO_3-Based Lead-Free Relaxor Ferroelectrics. *J. Eur. Ceram. Soc.* **2020**, *40*, 5466–5474. [CrossRef]
142. Li, D.; Zhou, D.; Wang, D.; Zhao, W.; Guo, Y.; Shi, Z. Improved Energy Storage Properties Achieved in (K,Na)NbO_3-Based Relaxor Ferroelectric Ceramics via a Combinatorial Optimization Strategy. *Adv. Funct. Mater.* **2022**, *32*, 2111776. [CrossRef]
143. Zhang, M.; Yang, H.; Yu, Y.; Lin, Y. Energy Storage Performance of K0.5Na0.5NbO3-Based Ceramics Modified by $Bi(Zn_{2/3}(Nb_{0.85}Ta_{0.15})_{1/3})O_3$. *Chem. Eng. J.* **2021**, *425*, 131465. [CrossRef]
144. Zhang, M.; Yang, H.; Lin, Y.; Yuan, Q.; Du, H. Significant Increase in Comprehensive Energy Storage Performance of Potassium Sodium Niobate-Based Ceramics via Synergistic Optimization Strategy. *Energy Storage Mater.* **2022**, *45*, 861–868. [CrossRef]
145. Feng, J.; Ye, S.; Wang, A.; Lu, X.; Tong, Y.; Li, G. Flexible Cellulose Paper-based Asymmetrical Thin Film Supercapacitors with High-Performance for Electrochemical Energy Storage. *Adv. Funct. Mater.* **2014**, *24*, 7093–7101. [CrossRef]
146. Zhao, J.; Xu, S.; Tschulik, K.; Compton, R.G.; Wei, M.; O'Hare, D.; Evans, D.G.; Duan, X. Molecular-Scale Hybridization of Clay Monolayers and Conducting Polymer for Thin-Film Supercapacitors. *Adv. Funct. Mater.* **2015**, *25*, 2745–2753. [CrossRef]
147. Zhang, W.; Ye, Q.; Fu, D.; Xiong, R. Optoelectronic Duple Bistable Switches: A Bulk Molecular Single Crystal and Unidirectional Ultraflexible Thin Film Based on Imidazolium Fluorochromate. *Adv. Funct. Mater.* **2017**, *27*, 1603945. [CrossRef]
148. Li, F.; Hou, X.; Wang, J.; Zeng, H.; Shen, B.; Zhai, J. Structure-Design Strategy of 0–3 Type $(Bi_{0.32}Sr_{0.42}Na_{0.20})TiO_3/MgO$ Composite to Boost Energy Storage Density, Efficiency and Charge-Discharge Performance. *J. Eur. Ceram. Soc.* **2019**, *39*, 2889–2898. [CrossRef]
149. Jayakrishnan, A.R.; Silva, J.P.B.; Kamakshi, K.; Annapureddy, V.; Mercioniu, I.F.; Sekhar, K.C. Semiconductor/Relaxor 0–3 Type Composites: A Novel Strategy for Energy Storage Capacitors. *J. Sci. Adv. Mater. Devices* **2021**, *6*, 19–26. [CrossRef]
150. Shi, J.; Chen, X.; Li, X.; Sun, J.; Sun, C.; Pang, F.; Zhou, H. Realizing Ultrahigh Recoverable Energy Density and Superior Charge–Discharge Performance in $NaNbO_3$-Based Lead-Free Ceramics via a Local Random Field Strategy. *J. Mater. Chem. C Mater.* **2020**, *8*, 3784–3794. [CrossRef]
151. Sun, Z.; Wang, Z.; Tian, Y.; Wang, G.; Wang, W.; Yang, M.; Wang, X.; Zhang, F.; Pu, Y. Progress, Outlook, and Challenges in Lead-Free Energy-Storage Ferroelectrics. *Adv. Electron. Mater.* **2020**, *6*, 1900698. [CrossRef]
152. Pan, H.; Li, F.; Liu, Y.; Zhang, Q.; Wang, M.; Lan, S.; Zheng, Y.; Ma, J.; Gu, L.; Shen, Y.; et al. Ultrahigh–Energy Density Lead-Free Dielectric Films via Polymorphic Nanodomain Design. *Science* **2019**, *365*, 578–582. [CrossRef] [PubMed]
153. Silva, J.P.B.; Silva, J.M.B.; Oliveira, M.J.S.; Weingärtner, T.; Sekhar, K.C.; Pereira, M.; Gomes, M.J.M. High-Performance Ferroelectric–Dielectric Multilayered Thin Films for Energy Storage Capacitors. *Adv. Funct. Mater.* **2019**, *29*, 1807196. [CrossRef]
154. Sun, N.; Li, Y.; Zhang, Q.; Hao, X. Giant Energy-Storage Density and High Efficiency Achieved in $(Bi_{0.5}Na_{0.5})TiO_3$–$Bi(Ni_{0.5}Zr_{0.5})O_3$ Thick Films with Polar Nanoregions. *J. Mater. Chem. C Mater.* **2018**, *6*, 10693–10703. [CrossRef]
155. Yang, C.; Lv, P.; Qian, J.; Han, Y.; Ouyang, J.; Lin, X.; Huang, S.; Cheng, Z. Fatigue-Free and Bending-Endurable Flexible Mn-Doped $Na_{0.5}Bi_{0.5}TiO_3$-$BaTiO_3$-$BiFeO_3$ Film Capacitor with an Ultrahigh Energy Storage Performance. *Adv. Energy Mater.* **2019**, *9*, 1803949. [CrossRef]
156. Yang, C.; Qian, J.; Han, Y.; Lv, P.; Huang, S.; Cheng, X.; Cheng, Z. Design of an All-Inorganic Flexible $Na_{0.5}Bi_{0.5}TiO_3$-Based Film Capacitor with Giant and Stable Energy Storage Performance. *J. Mater. Chem. A Mater.* **2019**, *7*, 22366–22376. [CrossRef]
157. Liang, Z.; Ma, C.; Shen, L.; Lu, L.; Lu, X.; Lou, X.; Liu, M.; Jia, C.-L. Flexible Lead-Free Oxide Film Capacitors with Ultrahigh Energy Storage Performances in Extremely Wide Operating Temperature. *Nano Energy* **2019**, *57*, 519–527. [CrossRef]

158. Liang, Z.; Liu, M.; Shen, L.; Lu, L.; Ma, C.; Lu, X.; Lou, X.; Jia, C.-L. All-Inorganic Flexible Embedded Thin-Film Capacitors for Dielectric Energy Storage with High Performance. *ACS Appl. Mater. Interfaces* **2019**, *11*, 5247–5255. [CrossRef]
159. Song, B.; Wu, S.; Li, F.; Chen, P.; Shen, B.; Zhai, J. Excellent Energy Storage Density and Charge–Discharge Performance of a Novel $Bi_{0.2}Sr_{0.7}TiO_3$–$BiFeO_3$ Thin Film. *J. Mater. Chem. C Mater.* **2019**, *7*, 10891–10900. [CrossRef]
160. Kursumovic, A.; Li, W.-W.; Cho, S.; Curran, P.J.; Tjhe, D.H.L.; MacManus-Driscoll, J.L. Lead-Free Relaxor Thin Films with Huge Energy Density and Low Loss for High Temperature Applications. *Nano Energy* **2020**, *71*, 104536. [CrossRef]
161. Sun, N.; Li, Y.; Liu, X.; Hao, X. High Energy-Storage Density under Low Electric Field in Lead-Free Relaxor Ferroelectric Film Based on Synergistic Effect of Multiple Polar Structures. *J. Power Sources* **2020**, *448*, 227457. [CrossRef]
162. Fan, Y.; Zhou, Z.; Chen, Y.; Huang, W.; Dong, X. A Novel Lead-Free and High-Performance Barium Strontium Titanate-Based Thin Film Capacitor with Ultrahigh Energy Storage Density and Giant Power Density. *J. Mater. Chem. C Mater.* **2020**, *8*, 50–57. [CrossRef]
163. Yang, C.; Qian, J.; Lv, P.; Wu, H.; Lin, X.; Wang, K.; Ouyang, J.; Huang, S.; Cheng, X.; Cheng, Z. Flexible Lead-Free BFO-Based Dielectric Capacitor with Large Energy Density, Superior Thermal Stability, and Reliable Bending Endurance. *J. Mater.* **2020**, *6*, 200–208. [CrossRef]
164. Qian, J.; Han, Y.; Yang, C.; Lv, P.; Zhang, X.; Feng, C.; Lin, X.; Huang, S.; Cheng, X.; Cheng, Z. Energy Storage Performance of Flexible NKBT/NKBT-ST Multilayer Film Capacitor by Interface Engineering. *Nano Energy* **2020**, *74*, 104862. [CrossRef]
165. Chen, J.; Tang, Z.; Yang, B.; Zhao, S. Ultra-High Energy Storage Performances Regulated by Depletion Region Engineering Sensitive to the Electric Field in PNP-Type Relaxor Ferroelectric Heterostructural Films. *J. Mater. Chem. A Mater.* **2020**, *8*, 8010–8019. [CrossRef]
166. Yang, C.; Han, Y.; Feng, C.; Lin, X.; Huang, S.; Cheng, X.; Cheng, Z. Toward Multifunctional Electronics: Flexible NBT-Based Film with a Large Electrocaloric Effect and High Energy Storage Property. *ACS Appl. Mater. Interfaces* **2020**, *12*, 6082–6089. [CrossRef]
167. Yang, X.; Li, W.; Zhang, Y.; Qiao, Y.; Yang, Y.; Fei, W. High Energy Storage Density Achieved in Bi^{3+}-Li^{+} Co-Doped $SrTi_{0.99}Mn_{0.01}O_3$ Thin Film via Ionic Pair Doping-Engineering. *J. Eur. Ceram. Soc.* **2020**, *40*, 706–711. [CrossRef]
168. Sun, Y.; Zhang, L.; Wang, H.; Guo, M.; Lou, X.; Wang, D. Composition-Driven Inverse-to-Conventional Transformation of Electrocaloric Effect and Large Energy Storage Density in Strontium Modified $Ba(Zr_{0.1}Ti_{0.9})O_3$ Thin Films. *J. Mater. Chem. C Mater.* **2020**, *8*, 1366–1373. [CrossRef]
169. Silva, J.P.B.; Silva, J.M.B.; Sekhar, K.C.; Palneedi, H.; Istrate, M.C.; Negrea, R.F.; Ghica, C.; Chahboun, A.; Pereira, M.; Gomes, M.J.M. Energy Storage Performance of Ferroelectric ZrO_2 Film Capacitors: Effect of HfO_2:Al_2O_3 Dielectric Insert Layer. *J. Mater. Chem. A Mater.* **2020**, *8*, 14171–14177. [CrossRef]
170. Zhang, Y.; Li, W.; Cao, W.; Feng, Y.; Qiao, Y.; Zhang, T.; Fei, W. Mn Doping to Enhance Energy Storage Performance of Lead-Free 0.7NBT-0.3ST Thin Films with Weak Oxygen Vacancies. *Appl. Phys. Lett.* **2017**, *110*, 243901. [CrossRef]
171. Zhang, Y.; Li, W.; Qiao, Y.; Zhao, Y.; Wang, Z.; Yu, Y.; Xia, H.; Li, Z.; Fei, W. 0.6ST-0.4NBT Thin Film with Low Level Mn Doping as a Lead-Free Ferroelectric Capacitor with High Energy Storage Performance. *Appl. Phys. Lett.* **2018**, *112*, 093902. [CrossRef]
172. Peng, B.; Zhang, Q.; Li, X.; Sun, T.; Fan, H.; Ke, S.; Ye, M.; Wang, Y.; Lu, W.; Niu, H.; et al. Giant Electric Energy Density in Epitaxial Lead-Free Thin Films with Coexistence of Ferroelectrics and Antiferroelectrics. *Adv. Electron. Mater.* **2015**, *1*, 1500052. [CrossRef]
173. Pan, H.; Ma, J.; Ma, J.; Zhang, Q.; Liu, X.; Guan, B.; Gu, L.; Zhang, X.; Zhang, Y.-J.; Li, L.; et al. Giant Energy Density and High Efficiency Achieved in Bismuth Ferrite-Based Film Capacitors via Domain Engineering. *Nat. Commun.* **2018**, *9*, 1813. [CrossRef]
174. Pan, H.; Lan, S.; Xu, S.; Zhang, Q.; Yao, H.; Liu, Y.; Meng, F.; Guo, E.-J.; Gu, L.; Yi, D.; et al. Ultrahigh Energy Storage in Superparaelectric Relaxor Ferroelectrics. *Science* **2021**, *374*, 100–104. [CrossRef] [PubMed]
175. Zhao, P.; Wang, H.; Wu, L.; Chen, L.; Cai, Z.; Li, L.; Wang, X. High-Performance Relaxor Ferroelectric Materials for Energy Storage Applications. *Adv. Energy Mater.* **2019**, *9*, 1803048. [CrossRef]
176. Sun, Z.; Ma, C.; Liu, M.; Cui, J.; Lu, L.; Lu, J.; Lou, X.; Jin, L.; Wang, H.; Jia, C. Ultrahigh Energy Storage Performance of Lead-Free Oxide Multilayer Film Capacitors via Interface Engineering. *Adv. Mater.* **2017**, *29*, 1604427. [CrossRef] [PubMed]
177. Wang, D.; Fan, Z.; Zhou, D.; Khesro, A.; Murakami, S.; Feteira, A.; Zhao, Q.; Tan, X.; Reaney, I.M. Bismuth Ferrite-Based Lead-Free Ceramics and Multilayers with High Recoverable Energy Density. *J. Mater. Chem. A Mater.* **2018**, *6*, 4133–4144. [CrossRef]
178. Wang, G.; Li, J.; Zhang, X.; Fan, Z.; Yang, F.; Feteira, A.; Zhou, D.; Sinclair, D.C.; Ma, T.; Tan, X.; et al. Ultrahigh Energy Storage Density Lead-Free Multilayers by Controlled Electrical Homogeneity. *Energy Environ. Sci.* **2019**, *12*, 582–588. [CrossRef]
179. Seo, I.; Kang, H.W.; Han, S.H. Recent Progress in Dielectric Materials for MLCC Application. *J. Korean Inst. Electr. Electron. Mater. Eng.* **2022**, *35*, 103–118.
180. Zhang, L.; Hao, X. Dielectric Properties and Energy-Storage Performances of $(1-x)(Na_{0.5}Bi_{0.5})TiO_3$–$xSrTiO_3$ Thick Films Prepared by Screen Printing Technique. *J. Alloys Compd.* **2014**, *586*, 674–678. [CrossRef]
181. Gao, F.; Dong, X.; Mao, C.; Liu, W.; Zhang, H.; Yang, L.; Cao, F.; Wang, G. Energy-Storage Properties $0.89Bi_{0.5}Na_{0.5}TiO_3$–$0.06BaTiO_3$–$0.05K_{0.5}Na_{0.5}NbO_3$ Lead-Free Anti-ferroelectric Ceramics. *J. Am. Ceram. Soc.* **2011**, *94*, 4382–4386. [CrossRef]
182. Cao, W.; Li, W.; Feng, Y.; Bai, T.; Qiao, Y.; Hou, Y.; Zhang, T.; Yu, Y.; Fei, W. Defect Dipole Induced Large Recoverable Strain and High Energy-Storage Density in Lead-Free $Na_{0.5}Bi_{0.5}TiO_3$-Based Systems. *Appl. Phys. Lett.* **2016**, *108*, 202902. [CrossRef]
183. Cao, W.; Li, W.; Zhang, T.; Sheng, J.; Hou, Y.; Feng, Y.; Yu, Y.; Fei, W. High-Energy Storage Density and Efficiency of $(1-x)$[0.94 NBT–0.06 BT]–xST Lead-Free Ceramics. *Energy Technol.* **2015**, *3*, 1198–1204. [CrossRef]

184. Cao, W.P.; Li, W.L.; Dai, X.F.; Zhang, T.D.; Sheng, J.; Hou, Y.F.; Fei, W.D. Large Electrocaloric Response and High Energy-Storage Properties over a Broad Temperature Range in Lead-Free NBT-ST Ceramics. *J. Eur. Ceram. Soc.* **2016**, *36*, 593–600. [CrossRef]
185. Mishra, A.; Majumdar, B.; Ranjan, R. A Complex Lead-Free (Na,Bi,Ba)(Ti,Fe)O_3 Single Phase Perovskite Ceramic with a High Energy-Density and High Discharge-Efficiency for Solid State Capacitor Applications. *J. Eur. Ceram. Soc.* **2017**, *37*, 2379–2384. [CrossRef]
186. Zhao, L.; Gao, J.; Liu, Q.; Zhang, S.; Li, J.-F. Silver Niobate Lead-Free Antiferroelectric Ceramics: Enhancing Energy Storage Density by B-Site Doping. *ACS Appl. Mater. Interfaces* **2018**, *10*, 819–826. [CrossRef] [PubMed]
187. Murakami, S.; Wang, D.; Mostaed, A.; Khesro, A.; Feteira, A.; Sinclair, D.C.; Fan, Z.; Tan, X.; Reaney, I.M. High Strain (0.4%) $Bi(Mg_{2/3}Nb_{1/3})O_3$-$BaTiO_3$-$BiFeO_3$ Lead-free Piezoelectric Ceramics and Multilayers. *J. Am. Ceram. Soc.* **2018**, *101*, 5428–5442. [CrossRef]
188. Cumming, D.J.; Sebastian, T.; Sterianou, I.; Rödel, J.; Reaney, I.M. Bi(Me)O_3–$PbTiO_3$ High T_C Piezoelectric Multilayers. *Mater. Technol.* **2013**, *28*, 247–253. [CrossRef]
189. Cross, L.E. Relaxor Ferroelectrics. *Ferroelectrics* **1987**, *76*, 241–267. [CrossRef]
190. Ma, C.; Tan, X. Phase Diagram of Unpoled Lead-Free—Ceramics. *Solid. State Commun.* **2010**, *150*, 1497–1500. [CrossRef]
191. Jabbari, M.; Bulatova, R.; Tok, A.I.Y.; Bahl, C.R.H.; Mitsoulis, E.; Hattel, J.H. Ceramic Tape Casting: A Review of Current Methods and Trends with Emphasis on Rheological Behaviour and Flow Analysis. *Mater. Sci. Eng. B* **2016**, *212*, 39–61. [CrossRef]
192. Kurchania, R.; Milne, S.J. Characterization of Sol-Gel $Pb(Zr_{0.53}Ti_{0.47})O_3$ Films in the Thickness Range 0.25–10 Mm. *J. Mater. Res.* **1999**, *14*, 1852–1859. [CrossRef]
193. Kishimoto, A.; Koumoto, K.; Yanagida, H.; Nameki, M. Microstructure Dependence of Mechanical and Dielectric Strengths—I. Porosity. *Eng. Fract. Mech.* **1991**, *40*, 927–930. [CrossRef]
194. Li, J.; Shen, Z.; Chen, X.; Yang, S.; Zhou, W.; Wang, M.; Wang, L.; Kou, Q.; Liu, Y.; Li, Q.; et al. Grain-Orientation-Engineered Multilayer Ceramic Capacitors for Energy Storage Applications. *Nat. Mater.* **2020**, *19*, 999–1005. [CrossRef] [PubMed]
195. Zhu, L.-F.; Deng, S.; Zhao, L.; Li, G.; Wang, Q.; Li, L.; Yan, Y.; Qi, H.; Zhang, B.-P.; Chen, J.; et al. Heterovalent-Doping-Enabled Atom-Displacement Fluctuation Leads to Ultrahigh Energy-Storage Density in $AgNbO_3$-Based Multilayer Capacitors. *Nat. Commun.* **2023**, *14*, 1166. [CrossRef]
196. Cai, Z.; Zhu, C.; Wang, H.; Zhao, P.; Chen, L.; Li, L.; Wang, X. High-Temperature Lead-Free Multilayer Ceramic Capacitors with Ultrahigh Energy Density and Efficiency Fabricated via Two-Step Sintering. *J. Mater. Chem. A Mater.* **2019**, *7*, 14575–14582. [CrossRef]
197. Gerson, R.; Marshall, T.C. Dielectric Breakdown of Porous Ceramics. *J. Appl. Phys.* **1959**, *30*, 1650–1653. [CrossRef]
198. Lu, Z.; Wang, G.; Bao, W.; Li, J.; Li, L.; Mostaed, A.; Yang, H.; Ji, H.; Li, D.; Feteira, A.; et al. Superior Energy Density through Tailored Dopant Strategies in Multilayer Ceramic Capacitors. *Energy Environ. Sci.* **2020**, *13*, 2938–2948. [CrossRef]
199. Hu, T.-Y.; Ma, C.; Dai, Y.; Fan, Q.; Liu, M.; Jia, C.-L. Enhanced Energy Storage Performance of Lead-Free Capacitors in an Ultrawide Temperature Range via Engineering Paraferroelectric and Relaxor Ferroelectric Multilayer Films. *ACS Appl. Mater. Interfaces* **2020**, *12*, 25930–25937. [CrossRef]